JOURNAL OF CHEMICAL INFORMATION AND MODELING

Article

pubs.acs.org/jcim

Structure−Activity Relationships in Non-Ligand Binding Pocket (Non-LBP) Diarylhydrazide Antiandrogens

Laura Caboni,[†] Billy Egan,[‡] Brendan Kelly,[†] Fernando Blanco,*[,†] Darren Fayne,[†] Mary J. Meegan,[‡] and David G. Lloyd[†,§]

[†]Molecular Design Group, School of Biochemistry and Immunology, Trinity Biomedical Sciences Institute, Trinity College Dublin, Dublin 2, Ireland

[‡]School of Pharmacy and Pharmaceutical Sciences, Trinity Biomedical Sciences Institute, Trinity College Dublin, Dublin 2, Ireland

[§]Division of Health Sciences, University of South Australia, Adelaide SA5000, Australia

Supporting Information

ABSTRACT: We report the synthesis and a study of the structure−activity relationships of a new series of diarylhydrazides as potential selective non-ligand binding pocket androgen receptor antagonists. Their biological activity as antiandrogens in the context of the development of treatments for castration resistant prostate cancer was evaluated using *in vitro* time resolved fluorescence resonance energy transfer and fluorescence polarization on target assays. Additionally, a theoretical study combining docking and molecular dynamics methods was performed to provide insight into their mechanism of action as a basis for further lead optimization studies.

INTRODUCTION

The androgen receptor (AR) is a relevant target in drug discovery involved in a variety of pathological processes such as androgen insensitivity syndrome (AIS), spinal bulbar muscular atrophy (SBMA), and prostate cancer (PCa).[1] Specifically, in PCa, androgens and androgen signaling through AR are required for both prostate development as well as cancer initiation and progression.[2,3]

AR is a member of the nuclear receptor (NR) superfamily, a class of ligand-activated transcription factors.[4] The mechanism of activation of AR involves the binding of natural androgens, like testosterone (T) and dihydrotestosterone (DHT), to the ligand binding domain (LBD). The LBD (Figure 1a) is highly structurally conserved throughout the NR superfamily, containing 12 α-helices that are folded into a typical three-layer helix sandwich, enclosing a hydrophobic region, constituting the ligand binding pocket (LBP). When the ligand binds to the LBP, helix 12 undergoes a conformational change generating a secondary hydrophobic region called activation function-2 (AF-2) on the surface of the protein suitable for the recruitment of coactivators and corepressors (Figure 1b).[5] More than 165 coactivators are known to interact with the AR alone.[6] The ligand-dependent AR-coactivator interaction modulates the transcriptional activity of AR, and deregulations at this interface - such as coregulator overexpression or acquired mutations - are frequently associated with prostate cancer.[7,8]

Traditionally, the mainstay for prostate cancer treatment has been androgen deprivation therapy (ADT),[10] typically achieved through chemical castration and mostly employing concurrent LBP directed intervention ('LBP' antiandrogens). These therapeutics bind to AR in the LBP, mimicking androgen's mode of action, but blocking the receptor's dynamic formation of the AF-2 coregulator region through the incorporation of specific bulky substituents that prevent the 'closure' of helix 12. A major drawback of this therapy is the development of drug resistance. Castration Resistant Prostate Cancer (CRPC) is frequently metastatic and almost invariably fatal. Recent studies have concentrated on this progression from an androgen-dependent and therapy-responsive stage to an androgen-independent, therapy-resistant stage.[11] One of the postulated molecular mechanisms of resistance to therapy relates to the intrinsic agonistic activity of the 'LBP' antiandrogens, which increase the transactivation potential of AR.[12] Due to these unfavorable limitations, recent efforts have concentrated on designing compounds that could overcome drug resistance in CRPC.[13,14] 'True' LBP antiandrogens like RD-162,[15] MDV-3100,[16,17] BMS-641988,[18,19] and the newly discovered ARN-509[20] are noteworthy among this class of inhibitors. An alternative approach is the design of non-LBP antiandrogens that could circumvent LBP related shortcomings. Recently, non-LBP strategies directly disrupting the interaction between the protein and its coactivator at AF-2 or at allosteric regulatory surfaces have been reported for AR[21,22] and other members of

Received: March 30, 2013
Published: July 8, 2013

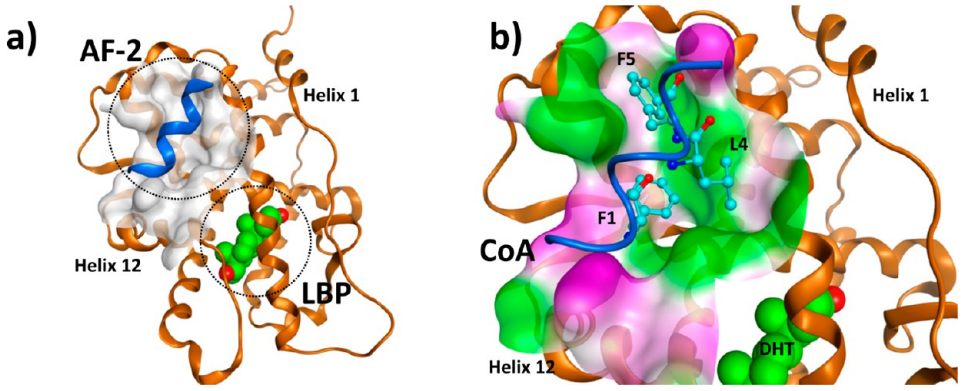

Figure 1. Crystal structure of the androgen receptor in complex with a FXXLF motif. a) Tertiary structure of AR ligand binding domain (LBD); b) Molecular surface rendering of AR activation function-2 (AF-2), *green* and *magenta* correspond to hydrophobic and polar regions, respectively. Images were generated using MOE.[9]

the family of nuclear receptors.[23] The viability of the non-LBP approach has also been documented for AR[21,24−29] where the interaction with coactivators has been blocked by both peptide antagonists[30,31] and small molecules.[21,26−28,32]

Regarding our search for alternative non-LBP therapeutics against CRPC, in two previous articles we described a series of diarylhydrazides as potential antiandrogens identified using a virtual screening approach. A number of derivatives were chemically characterized and subjected to biological evaluation.[33,34] Among these derivatives, compounds **1**−**5** (Figure 2) showed AR antagonistic activity by TR-FRET analysis, and a non-LBP mechanism of action was confirmed by FP assays. Interestingly, many other derivatives of the same family were inactive (**6**−**25**) under identical conditions. Accordingly, we considered it necessary to conduct a more detailed structure−activity relationship study, which we present here. Additionally, a theoretical study (docking and molecular dynamics) was performed in order to further rationalize our results and provide new insights into the potential binding mode of these systems within the AR AF-2 for the design of subsequent families of inhibitors with enhanced biological profiles.

RESULTS AND DISCUSSION

Structural Basis of AR-Antagonism by Diarylhydrazides. Figure 2 shows a selection of diarylhydrazides reported in our previous work. Of these compounds, five derivatives were identified and characterized as non-LBP AR-antagonists (**1**−**5**). However, these data show that small differences in the substitution patterns on the main scaffold produce dramatic effects on the activity. Building on these initial observations, a second generation of derivatives was designed.

An initial SAR analysis of our systems provided us with the following key points that guided the synthesis of new candidates (see Figure 3): a) *Naphthyl vs Phenyl Functionality at Rings A and B:* It was observed that naphthyl decoration at ring A provides active ligands. Substitution with a phenyl ring (**4** vs **23**) abolishes the activity. Conversely, both phenyl (**1**−**4**) and naphthyl (**5**) functionality at the ring B position lead to active ligands; b) *OH Substitution on Ring A:* Most of the compounds evaluated, including the five active ones, contain an OH group at the C3 position of naphthyl ring A. Methylation at this position (**22**) eliminates the AR antagonistic activity, suggesting that the hydrogen of the hydroxyl group could be essential for activity; and c) *OH Substitution on Ring B:* Almost all of the active compounds (**2**−**5**) have a hydroxyl group on ring B located *ortho* to the linker (C2′ or C3′ for phenyl and naphthyl rings respectively), and it was demonstrated that removal of this OH group abolishes the activity (**5** vs **7**). Moreover, none of the other substituents evaluated at this position (CH_3, Cl, and COOH) provided active ligands (**11**, **12**, and **21**). The results also suggest that the contributory effect of the OH group occurs specifically when it occupies the C2′ position (phenyl ring), since derivatives hydroxylated in other positions (C3′ and C4′) were not active (**16**−**19**).

Synthesis of Diarylhydrazides. New (*E*)-*N*′-benzylidene-2-naphthohydrazide analogues (Figure 4) were synthesized following our previously reported standard procedure (Scheme 1):[34] esterification of 3-hydroxy-2-naphthoic acid (**I**) in the presence of methanol and hydrochloric acid, treatment of the resulting ester intermediate **II** with hydrazine hydrate producing hydrazide **III**, and condensation of **III** with the appropriate aldehyde to afford the products (**IV**) in good yields. Under these conditions, the *E*-isomer of the C═N is obtained almost quantitatively, as it was proven by a spectroscopic and theoretical study.[34]

Biological Evaluation of AR Modulation. *Measurement of AR Antagonistic Activity - AR TR-FRET Assays.* Diarylhydrazides **26**−**45** were subjected to AR TR-FRET experiments to determine their activity as AR antagonists. This technique evaluates the ability of the compounds to inhibit the recruitment of the fluorescently labeled D11-FXXLF coactivator peptide in the presence of an agonist (DHT) at a concentration equal to the EC_{80}. Results of these assays are gathered in Table 1. For those compounds that showed antagonist activity (**28**, **31**−**34**, and **36**−**38**), IC_{50} values were determined from 12-point dose−response curves (Figure 5a).

Determination of Non-LBP Mechanism of Action - AR FP Assays. Since the TR-FRET assay cannot differentiate between direct disruptors of coactivator binding (non-LBP antagonists) acting on the LBD surface and classical AR modulators (LBP antagonists) acting at the ligand binding pocket, active compounds were tested for their ability to displace a fluorescently labeled AR ligand (Fluormone) from the AR LBP. Compounds were assayed at a single point concentration (50 μM) using cyproterone acetate (CPA) as a reference, a known AR LBP antagonist. As illustrated in Figure 5(b), none of the compounds tested showed any statistically significant inhibition of the AR-LBD: Fluormone complex, indicating a non-LBP based mechanism.

dx.doi.org/10.1021/ci400189m | J. Chem. Inf. Model. 2013, 53, 2116−2130

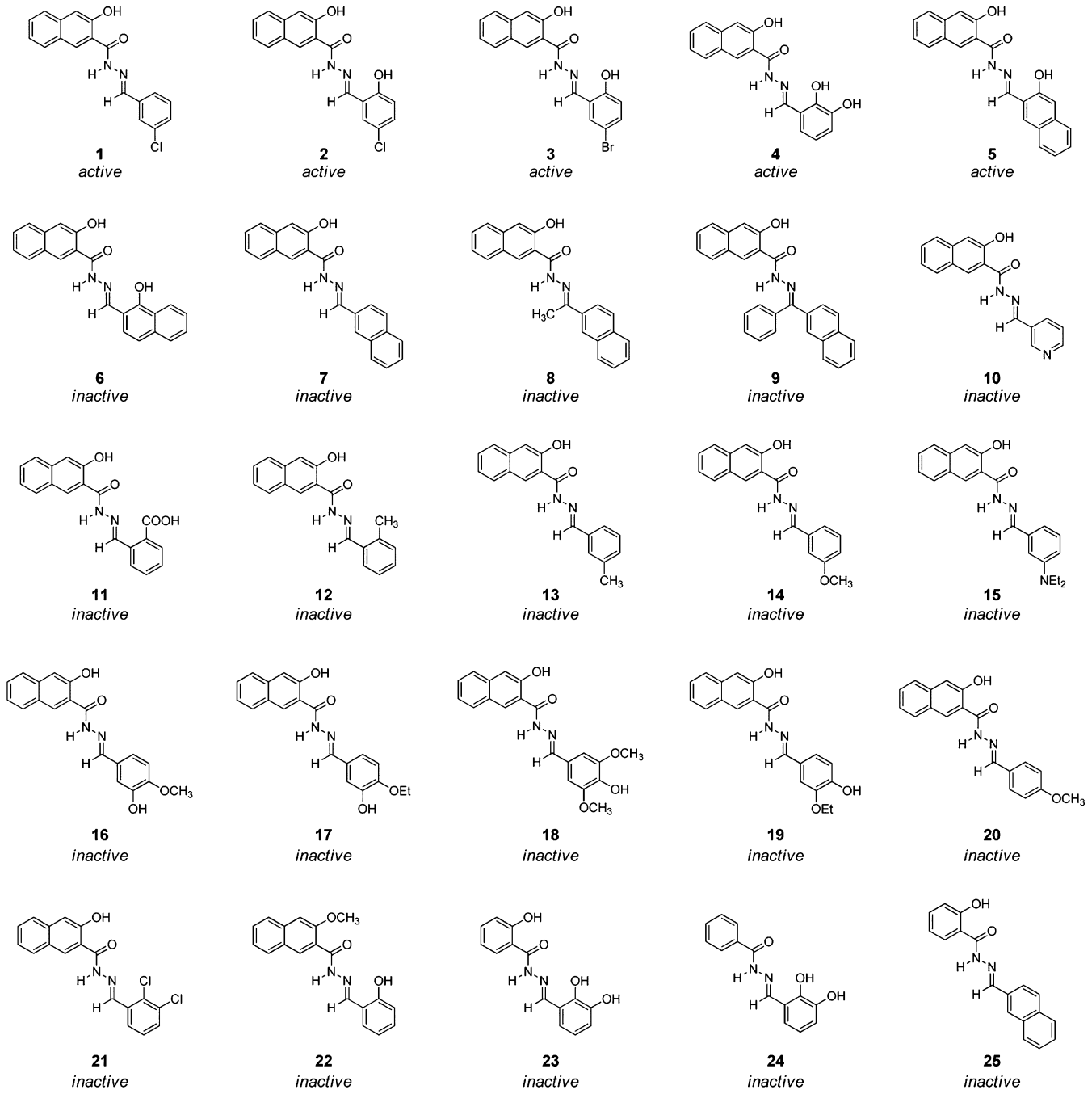

Figure 2. Diarylhydrazides: selection of analogues previously evaluated as AR antagonists. Compounds **1**−**5** were characterized as non-LBP 'true' antiandrogens with an IC_{50} in the low micromolar range (10−50 μM). Compounds **6**−**25** did not display antiandrogen activity (IC_{50} >100 μM).

Structure−Activity Relationship Study. Analysis of the biological results has provided interesting SAR patterns that can be summarized in seven main groups (Note: The following discussion is focused uniquely on phenyl B derivatives, meaning the numbering corresponds exclusively to this subfamily):

No Interchangeability of Aromatic Ends. As described before, despite the apparent level of molecular symmetry of our compounds - two aromatic rings joined by a linker - the two ends are not interchangeable. Replacement performed on ring A and B - substitution of a naphthyl group by a phenyl one - produces an opposite effect in activity. While in the case of B the antagonist character is maintained for this substitution (**5** and **28**), in A the antagonist activity is abolished (**4** vs **23**). This suggests that the ligands adopt a consistent conformation in the binding site; the two aromatic ends A and B seem to be accommodated in a specific orientation, in support of our AF-2 binding hypothesis.

Requirement for OH in the C3 Position of Naphthyl Ring A. The results confirm unambiguously the important role played by the hydroxyl function. Both removal (**2** vs **26**) and methylation (**28** vs **22**) of this group lead to the elimination of antagonistic effects. The key factor seems to be the availability of the hydrogen to participate in hydrogen bond (HB) interactions. *A priori*, it is most likely that these interactions occur between the ligand and the amino acids of the site (*Intermolecular Hypothesis*). However, considering the geometry

dx.doi.org/10.1021/ci400189m | J. Chem. Inf. Model. 2013, 53, 2116−2130

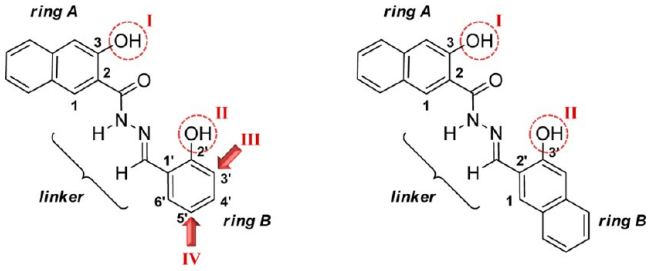

Figure 3. Diarylhydrazides: general structure and SAR guidelines. I. Significance of OH group in the C3 position of ring A; II. Significance of OH group in the C2′/C3′ position of ring B (for phenyl/naphthyl analogues respectively); III. Substitution effects at the C3′ position of ring B and IV. Effect of substituents at position C5′ of ring B.

of our molecules, a second valid hypothesis is that this hydrogen is involved in an intramolecular hydrogen bond (IMHB) with one of the groups of the linker which holds lone pairs (O_{CO} and N_{CN}), conferring rigidity to the system which could be necessary to adopt the bioactive conformation (*Intramolecular Hypothesis*).

Relevance of OH in the C2′ Position of Phenyl Ring B. The newly synthesized examples highlight the importance of the hydroxyl group on ring B, *ortho* to the linker. With only one exception (**1**), all active compounds contain this substituent (**2**−**5**, **28**, **31**−**34**, **36**−**38**). Similarly to what was observed with ring A, methylation of this group results in loss of activity (**28** vs **41** and **3** vs **42**), which leads to the same hypothesis relating to the role of the hydrogen atom. This hydrogen could be involved in HB interactions with the pocket (*Intermolecular Hypothesis*) or contribute to conferring rigidity to the ligands through interactions with the linker-hydrazone nitrogen's lone-pair of electrons (*Intramolecular Hypothesis*).

Substitution Effects at Position C2′ of Phenyl Ring B - 2′-Substituted Series. In addition to OH, we have studied six different functionalities on C2′ with different electronic profiles (CO_2H, CH_3, Cl, OCH_3, NO_2, and NH_2), none of which were active (**11**, **12**, **21**, **41**−**45**). Despite the fact that it is not possible to establish a clear pattern based on the electronics of the phenyl ring, the result reinforces the necessity for the OH substituent in this position.

Substitution Effects at Position C3′ of Phenyl Ring B - 2′-Hydroxy-3′-Substituted Series. The functionalization of C3′

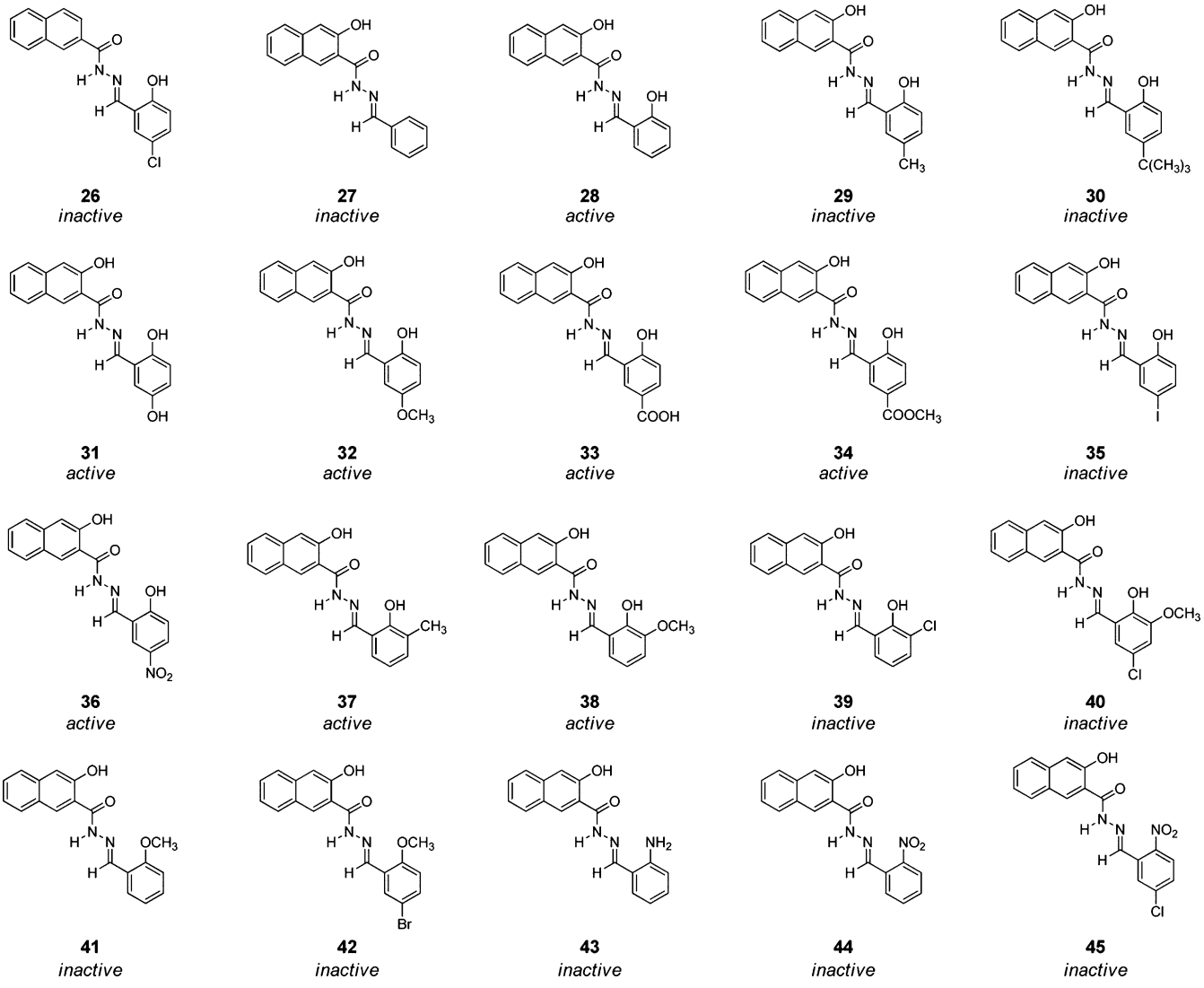

Figure 4. Diarylhydrazides: new series of synthesized analogues.

dx.doi.org/10.1021/ci400189m | J. Chem. Inf. Model. 2013, 53, 2116−2130

Scheme 1. Standard Method for the Synthesis of Diarylhydrazides

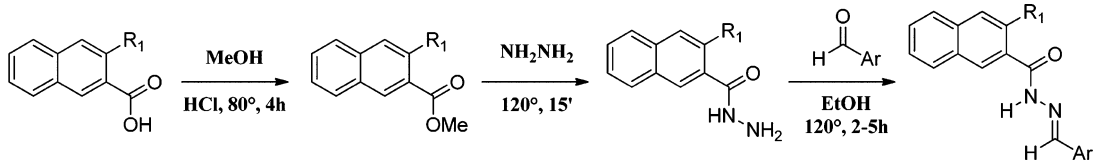

Table 1. Quantification of the AR-Antagonism of Diarylhydrazides by AR TR-FRET Assays

compd	IC_{50} (μM)[a]	compd	IC_{50} (μM)[a]
26	*NA*	**36**	*33.4 ± 4.7*
27	*NA*	**37**	*13.2 ± 2.8*
28	*55.2 ± 19.2*	**38**	*12.2 ± 0.5*
29	*NA*	**39**	*NA*
30	*NA*	**40**	*NA*
31	*39.9 ± 16.9*	**35**	*NA*
32	*53.0 ± 13.5*	**42**	*NA*
33	*43.5 ± 3.7*	**43**	*NA*
34	*60.7 ± 20.0*	**44**	*NA*
35	*NA*	**45**	*NA*

[a]All assays were performed in triplicate; the values represent the average of the three assays. Compounds with IC_{50} >100 μM were considered inactive (*NA = not active*).

provides the following results: 1. Compounds **37** and **38** (2′-hydroxy-3′-methyl- and 2′-hydroxy-3′-methoxyderivatives) are active within a similar range (IC_{50} = 12.3 and 13.2 μM respectively), improving significantly on the IC_{50} value of the 3′-unsubstituted analogue **28** (IC_{50} = 55.2 μM); 2. Compound **39** (2′-hydroxy-3′-chloroderivative) is inactive.

Substitution Effects at Position C5′ of Phenyl Ring B - 2′-Hydroxy-5′-Substituted Series. The functionalization of C5′ is the SAR feature that we have explored most extensively, due in part to its synthetic feasibility; there are more commercially available aldehydes with this position substituted than any other. Eleven derivatives were evaluated with the following substituents: H (**28**), CH_3 (**29**), tBu (**30**), OH (**31**), OCH_3 (**32**), CO_2H (**33**), CO_2CH_3 (**34**), Cl (**2**), Br (**3**), I (**35**), and NO_2 (**36**). Consistently, inductive electron-withdrawing groups (OH, OCH_3, CO_2H, CO_2CH_3, Cl, Br, and NO_2) provide active analogues and, electron-donating ones (CH_3 and ^tBu) or poorly withdrawing groups (I) abolish the activity. We could conclude that the electronic profile of the substituent at C5′ is a key determinant of activity in this system. Speculatively, the positive contribution exerted by such substituents could be due to i) their interaction with suitable regions within the AF-2 pocket (*direct effect*) or ii) the withdrawal of electronic density from the aromatic ring (*indirect effect*).

Methylation of Hydroxyl Groups. The effects arising from the substitution of hydroxyl groups by methoxy ones have been treated in some of the preceding points; however, it merits greater discussion in the context of these compounds. It has been clearly established that OH groups at positions C3 and C2′ are essential for AR activity. Considering that the hydroxyl and methoxy functions share a similar electronic profile, the fact that the methoxy group eliminates the antagonist character can be explained by either direct steric effects or - as suggested above - because the HB donor hydrogen of the OH is indispensable. Significantly, the methoxylation of other positions C3′ (**4** and **38**) and C5′ (**31** and **32**) does not affect the activity of compounds, emphasizing the concept that our ligands interact through a well-defined bioactive conformation.

As a general conclusion, we have developed a new family of antiandrogen ligands which interact with AR adopting a consistent conformational arrangement and disrupting the binding of the coactivator. These interactions have been interrogated with classical SAR expansion through synthesis and assay. In the absence of confirmation by crystallization, there is sufficient supporting evidence that these systems could bind, as designed, in the AF-2 region. In this context, we deemed it appropriate to explore a combination of docking and molecular dynamics simulations to substantiate the proposed AF-2 binding site.

Molecular Modeling of Diarylhydrazides in AR AF-2. The interaction of coactivators within the AF-2 groove occurs

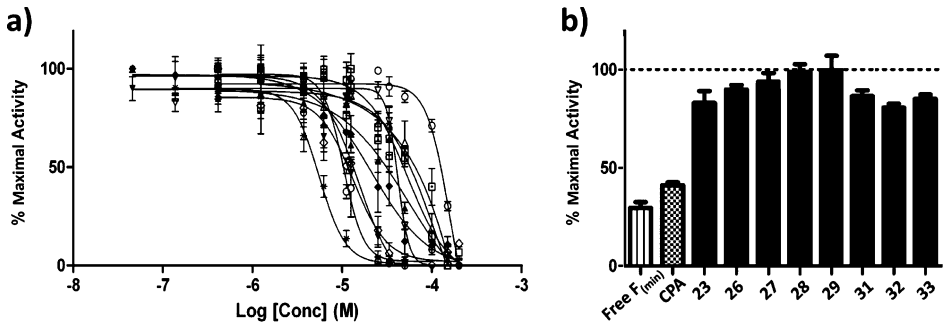

Figure 5. Biological characterization of active ligands (**28**, **31**−**34**, and **36**−**38**). a) TR-FRET dose response curves: compounds were tested in a TR-FRET assay across a concentration range from 45 nM to 100 μM, where applicable in the presence of a concentration of DHT = EC_{80} in AR-LBD wt. Data points represent the mean of two independent experiments performed in triplicate. Error bars represent the standard error of the mean (SEM) for n = 6 values. Data were fitted using Log antagonist concentration vs response (variable slope) with GraphPad Prism 5. b) FP data: fluorescence polarization data are plotted as % Maximal Activity represented by the AR-LBD and fluorophore complex (0% inhibition). Minimum control value represents free fluorophore (Free F) in solution (100% inhibition). Error bars represent the SEM for n = 6 values.

dx.doi.org/10.1021/ci400189m | J. Chem. Inf. Model. 2013, 53, 2116−2130

via the so-called 'NR box',[35] a peptide motif of 5 amino acids largely conserved across the NR coactivator superfamily. In general, most of the NRs accommodate coactivators with an LXXLL motif, where *L* represents a leucine and X represents any amino acid. However, AR has a greater specific preference toward the binding of phenylalanine-enriched motifs like FXXLF, as has been documented and supported by phage analysis and X-ray crystallographic data.[36,37] The AF-2 interface is divided into three hydrophobic subpockets (Figure 6a). In

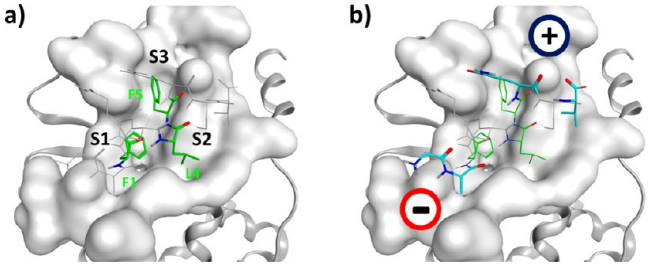

Figure 6. Structural and chemical features of the AR AF-2:coactivator (FXXLF) interaction. a) Molecular surface of AR showing the three hydrophobic subpockets ($F_1XXL_4F_5$ *motif highlighted in green*); b) Molecular surface of AR showing the AF-2 polar regions. Images were generated using MOE.[9]

the specific case of $F_1XXL_4F_5$, the residues F_1 and F_5 are accommodated in subpockets S1 and S3, respectively. As mentioned, all the subpockets are mainly hydrophobic; however, S1 and S3 are deeper grooves, while S2 appears to be flatter in shape and more exposed to solvent. S1 is clearly wider than S3, meaning it can potentially accommodate larger groups, while S3 is narrow and could cause major steric clashes with potential ligands. Furthermore, there are two polar regions flanking the site (the so-called *charge clamps*), the first being positive and located on top in between S2 and S3, the second being negative and at the bottom adjacent to S1 (Figure 6b).

In order to interrogate the most probable binding mode of diarylhydrazides, a theoretical study combining docking and molecular dynamics methods was performed following the protocol depicted in Figure 7. The following structures were specifically chosen to carry out the study (Figure 8): Compound **28** was selected as the active compound of reference, subsequently **27**, **46**, and **47** were selected to

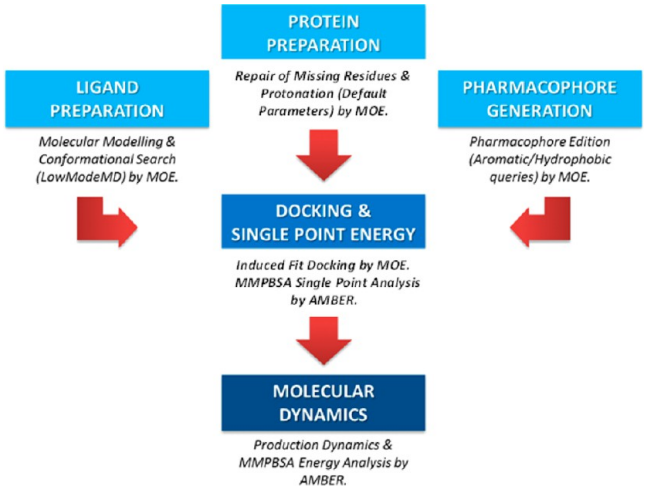

Figure 7. Theoretical study workflow.

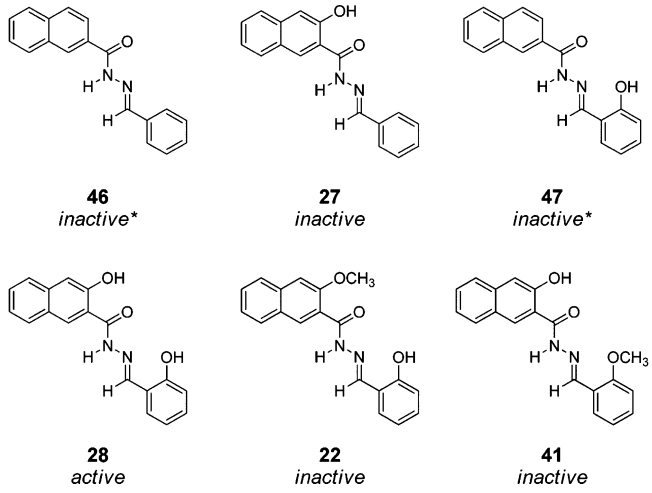

Figure 8. Structures selected for molecular modeling.

evaluate the effect of removal of OH groups, and **22** and **41** were chosen to evaluate the effect of methoxylation on critical positions C3 and C2′.

*Induced Fit Docking of Compound **28** and Its Related Analogues **46**, **27**, **47**, **22**, and **41** in Complex with AR AF-2.* General docking results are gathered in Table 2. The number of poses obtained for each evaluated structure was in the range 16−19. Scoring values were inconclusive to make assumptions about the mode of interaction of the ligands within AF-2. However, an analysis of the percentage of distribution of rings A and B into the AF-2 subpockets throughout the docking (*i.e.*, the ratio between the number of occurrences of a ring A or B in a specific subpocket divided by the total of poses) provided valuable information (Table 2). Results evidence the clear trend of ring A (naphtyl) to occupy S1 and of ring B (phenyl) to occupy S3 (**46**, **27**, **47**, and **28**). Both the length and geometry of the linker are suited to orient these rings to fill the subpockets S1 and S3, respectively, mimicking the known binding mode of the FXXLF coactivator motif and optimizing the hydrophobic interactions. Moreover, the introduction of methoxy groups significantly breaks this trend for ring A (**22** and **41**), which could be linked to the observed inactivity. Compound **28** was further investigated, as a representative of the active ligand series.

*MMPBSA Rescoring and Pose Analysis of Compound **28**.* Docking of **28** furnished 16 different binding poses. In order to filter unreasonable conformations, all of these poses were minimized and rescored by applying a standard MMPBSA protocol implemented in AMBER (see the Experimental Section). Table 3 lists the docking scores of the ligand-protein complexes and their 'single point' binding energies extracted from the MMPBSA analysis after minimization. Poses are ranked as a function of their docking score from **P1** to **P16**. ΔG(sp) represents the solvation free energies calculated by solving the linearized Poisson−Boltzmann equation. Although the scores (*S*) were not in good correlation with ΔG(sp) energies, the ranking of the poses provided by docking was quite reasonable, detecting up to seven of the energetically most favorable conformations among the top ten with 'better' binding values.

We selected six minimized poses of **28** (**P1**, **P3**, **P4**, **P6**, **P12**, and **P16**) based on the most favorable values of ΔG(sp) for further investigation (Table 3). The visual analysis of their geometries into the AF-2 pocket provided the following initial

dx.doi.org/10.1021/ci400189m | J. Chem. Inf. Model. 2013, 53, 2116−2130

Table 2. Docking Results of Compounds 46, 27, 47, 28, 22, and 41

			ring A distribution (%)			ring B distribution (%)		
compd	docking poses	scoring range	S1	S2	S3	S1	S2	S3
46	19	−24.1, −9.9	**63**	11	26	11	28	**61**
27	19	−24.7, −16.6	**53**	11	37	11	42	**47**
47	18	−25.1, −19.7	**72**	17	11	11	17	**72**
28	16	−25.1, −19.7	**56**	19	25	19	25	**56**
22	19	−27.1, −18.1	30	30	**40**	11	32	**58**
41	18	−25.0, −19.6	33	**44**	22	11	28	**61**

Table 3. Docking and MMPBSA Binding Energies of Compound 28 (kcal mol^{-1})

pose	*S*	Δ*G*(sp)	Δ*G* (40 ns)	stability of the pose[a]
P1	**-25.1**	**-16.0**	**-24.2**	***high***
P2	−24.7	−12.3	---	---
P3	−23.9	−18.6	−20.4	*medium*
P4	−23.7	−20.8	−19.3	*medium*
P5	−22.7	−4.5	---	---
P6	−22.2	−16.5	−19.2	*medium*
P7	−21.8	−9.6	---	---
P8	−21.4	−15.0	---	---
P9	−20.9	−15.1	---	---
P10	−20.8	−14.6	---	---
P11	−20.6	−15.1	---	---
P12	−20.5	−15.7	−14.0	*low*
P13	−20.3	−13.7	---	---
P14	−20.2	−10.2	---	---
P15	−19.8	−12.5	---	---
P16	−19.7	−19.7	−20.5	*low*

[a]Conformational stability of the poses has been evaluated as a function of its trend to keep a relatively constant shape and placement throughout the dynamics simulation.

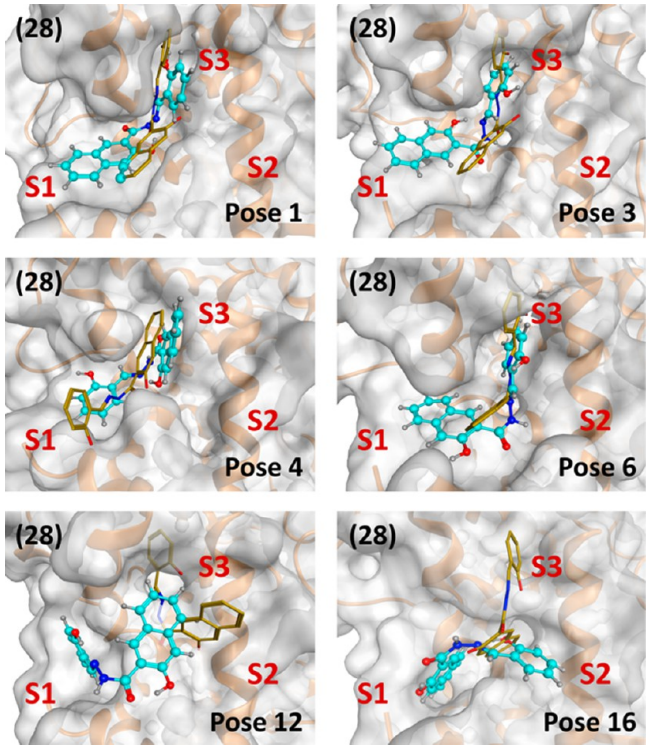

Figure 9. Selection of top ranked poses of (*E*)-3-hydroxy-*N*′-(2-hydroxybenzylidene)-2-naphthohydrazide **28**. Before and after conformations over the 40 ns of production dynamics are represented in *yellow* and *blue*, respectively. Images were generated using MOE.[9]

insights: a) **P1**, **P3**, and **P6** shared the aforementioned most favorable combination A-S1/B-S3, differing only in the orientation of rings A/B (OH groups pointing to the solvent or to the site). This arrangement places the bigger naphthyl ring A into the major groove (S1) and the phenyl ring B into the narrower S3, leaving the most exposed subpocket (S2) free; b) In **P4**, S1 and S3 were also occupied, but the distribution of the rings was swapped to B-S1/A-S3; and c) the **P12** conformation showed an A-S1/B-S2 distribution, which seemed to be less favorable considering the Δ*G*(sp) binding energies.

Molecular Dynamics of Selected Poses and Binding Energies. A production dynamics simulation of 40 ns duration was carried out to evaluate the stability and strength of these selected poses. As can be seen in Figure 9 (cf. *before* and *after* conformations), **P1** maintained a relatively constant shape and placement after 40 ns of production dynamics. **P3** and **P4** suffered internal rotation of A/B rings but maintained the A-S1/B-S3 placement. **P6** evolved from the initial pose to a better conformation by rotation of ring A, accommodating the naphthyl moiety on S1. **P12** and **P16**, meanwhile, evolved to a different pose far displaced from the original one. We considered as high, medium, or low the conformational stability of the analyzed poses of the ligand in the pocket (Table 3), **P1** clearly being the most stable conformation.

The final calculated binding energies after dynamics simulation are presented in Table 3. Δ*G*(40 ns) correspond to the average values over the last 5 ns of production dynamics when the geometry and Δ*G* of the complexes are stabilized. The results ranked **P1** and **P3** (−24.2 and −20.4 kcal mol^{-1}, respectively) as the conformations with the strongest interaction energies, followed by **P4** (−19.3 kcal mol^{-1}). **P6** evolved to a **P3** type arrangement (−19.2 kcal mol^{-1}), confirming the better suitability of S1 and S3 to accommodate rings A and B, respectively. Finally, **P12** and **P16** were not stable poses; thus, their binding energies are not representative and were not considered.

The theoretical descriptors (docking scores, stability of the pose, and MMPBSA values) confirmed **P1** as the most probable bioactive conformation adopted by our active ligand **28** at the AF-2 site, so this pose was studied more in depth.

MMPBSA Energy Decomposition Analysis of the Proposed Bioactive Conformation P1. The MMPBSA protocol implements a 'pair wise' method to analyze the independent contribution of each amino acid to the binding interaction with the ligand, allowing the detection of which residues are specifically involved and have a more significant influence on the global binding process. Figure 10 collates the energy

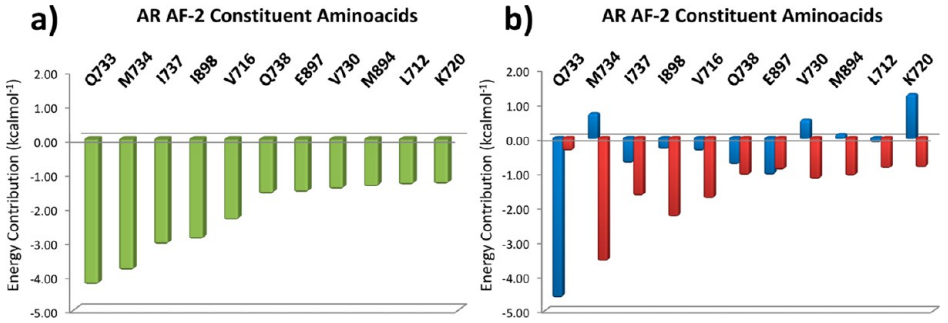

Figure 10. 'Pair wise' energy decomposition analysis by MMPBSA. a) Total energy contribution of the most relevant amino acids; b) Electrostatic (*blue*) and van der Waals (*red*) energy contribution to the binding.

contribution of the residues of the receptor (AR AF-2 site) that participate in the interaction with **28**.

As can be seen, the most significant contribution corresponds to Q733 placed in S3 and M734, which is located in the 'border' region between S1 and S3 (Figure 11), followed by

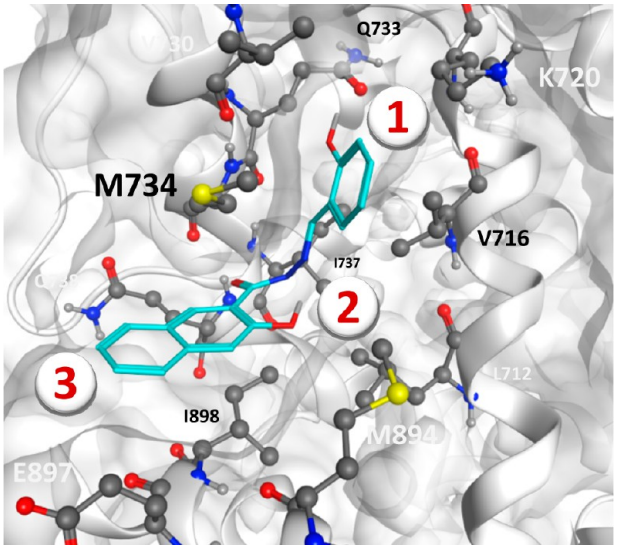

Figure 11. Selection of main protein:ligand interacting points in P1. 1. Highly contributory hydrogen bond interaction between $OH_{C2'}$ and Q738 on S3; 2. Favorable internal rearrangement of ligand **28** by stabilizing intramolecular hydrogen bond between OH_{C3} and N_{CN}; 3. High occupancy of subpocket S1 by naphthyl moiety A through hydrophobic stabilization. Images were generated using MOE.[9]

I737, I898, Q738 and E897 (S1), and V730 (S3) and to a lesser extent by M894, L712 (S2), and K720 (S2/S3 border). The decomposition of the energy contribution into its two fundamental components (electrostatic and van der Waals) suggests that, while the interaction of the ligand with glutamine Q733 is governed by electrostatic forces (corresponding with ionic bonds or hydrogen bond interactions), in the remaining amino acids the van der Waals component (related to hydrophobic interactions) is the more influential. Indeed, as explained before, in **P1** the phenyl ring B is accommodated in S3 with the $OH_{C2'}$ oriented to the pocket, such that the hydrogen forms an intermolecular HB with Q733. This interaction largely explains the electrostatic character of its contribution. Simultaneously, the rest of the structure of the ligand is arranged longitudinally in the proximity of M734, I898, and I737 among others, with the naphthyl group occupying the maximum volume possible of S1, optimizing the hydrophobic interactions (Figure 11, points 1 and 3). On the other hand, the secondary hydroxyl group OH_{C3} is not interacting directly with any amino acid in the pocket; however, it is oriented such that it stabilizes the geometry of the ligand through an IMHB with the imine nitrogen of the linker (Figure 11, point 2). This internal rearrangement of the ligand places the carbonyl group in the surroundings of the amino groups of the backbone of residues I737 and Q738 interacting by a weak hydrogen bond, a fact that is reflected in a small electrostatic contribution (Figure 10b). With this in mind, it is relatively easy to understand why certain hydroxyl groups are essential for antagonist activity and, moreover, why methoxylation at these positions produces such negative consequences on the effectiveness of compounds.

To further evaluate these hypotheses we decided to simulate our elected pose (**P1**) as applied to the previously selected analogues (**46**, **27**, **47**, **22**, and **41**), in order to have a complete description of the problem under discussion.

Role of OH Groups in the Bioactive Conformation and Consequences of Methoxylation. One of the clear conclusions of our SAR investigation was the key role played by the OH groups on positions C3 and C2′ in conferring antagonist character to our ligands. The proposed bioactive conformation **P1** rationalizes this observation, since both groups are relevant for its particular interaction with the AF-2 site. OH_{C3} is located in proximity to the imine lone pair (N_{CN}), conferring certain stability to the geometry of the ligand, and, more significantly, $OH_{C2'}$ interacts directly with the pocket through an intermolecular HB with glutamine Q733 as previously explained. Considering this, it was expected that either the removal or methylation of these OH groups would have a negative influence on binding, which, should our simulation hypothesis hold true, would be reflected in some way by MD analysis. Figure 12 shows the *before* and *after* geometries of the simulated **P1** conformation for compounds **46**, **27**, **47**, **28**, **22**, and **41** after 40 ns of production dynamics (Note: *We assume the existence of other favorable poses for these ligands; however, for the purpose of this study we only focused on the effects derived from the presence/absence of OH groups and its methylation specifically on the stability of the hypothetic bioactive conformation* ***P1***.). It is evident that the results highlight the proposed role of the hydroxyl groups in conferring activity to this class of ligands. OH containing derivatives **27** and **28** remain in the pocket throughout the entire production period, while monohydroxylated derivative **47** is partially maintained in the pocket thanks to the strength of the binding interaction of the phenyl moiety with S3. The nonhydroxylated derivative **46**, however, is not able to maintain its position in the site in these simulations.

dx.doi.org/10.1021/ci400189m | J. Chem. Inf. Model. 2013, 53, 2116−2130

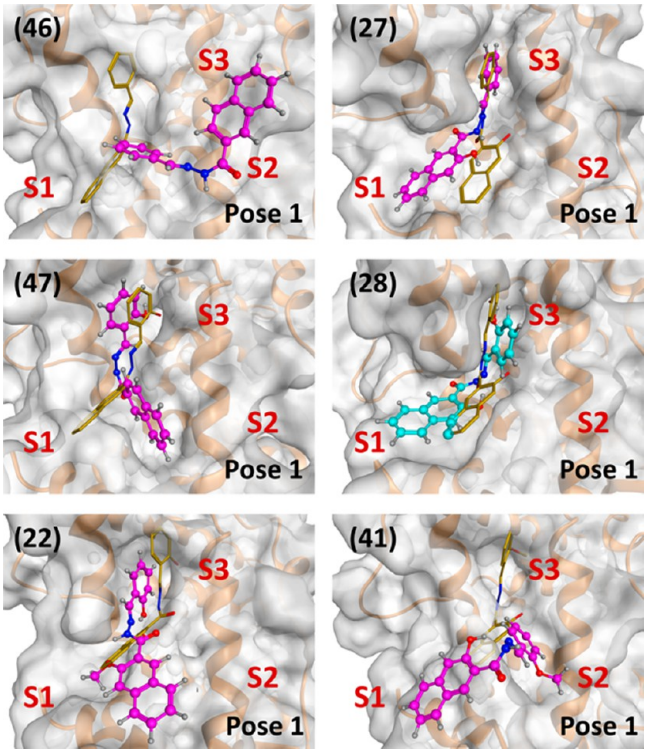

Figure 12. Role of hydroxylation and methoxylation: effect on bioactive conformation P1 (MD study). Before and after conformations over the 40 ns of production dynamics are represented in yellow and magenta, respectively. Images were generated by MOE.[9]

The negative effect on binding caused by the introduction of methoxy groups is also evidenced by the two representative analogues **22** and **41**; they are expelled from the site due to both the disruption of the aforementioned interacting points and the introduction of steric clashes caused by the presence of the methoxy moiety. All of these results are in good agreement with our hypothesis and the reported SAR observations supporting the designation of **P1** as the most probable bioactive conformation.

Based on all of this evidence, we propose that the design of future new candidates in this class of compound must incorporate the functionalization of key positions in the diarylhydrazide skeleton which increase the ability of this class of ligand to bind strongly to the AF-2 region while conserving the OH moieties which confer activity. These functionalizations consist of the introduction of substituents capable of interacting with the previously described charged regions (negative or positive groups in the proximity of K720 or E897, respectively) as well as the evaluation of new linkers that could exploit the availability of subpocket S2 (Figure 13).

CONCLUSIONS

A new series of 20 diarylhydrazides has been synthesized and evaluated for AR antagonist activity. Eight of these novel compounds have shown antiandrogen activity by a proven non-LBP mechanism of action, an intriguing approach that might lead to treatments for castration resistant prostate cancer.

Structure−activity relationships have been established which highlight the fundamental role played by hydroxyl substituents in critical positions within the diarylhydrazide scaffold and the negative effects brought about by their removal or methylation. Further SAR observations have provided a deeper understanding of the main parameters that determine the effectiveness of these compounds as AR antagonists.

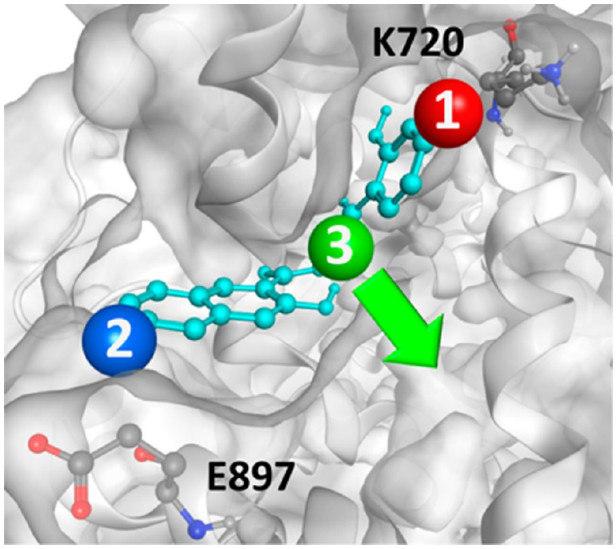

Figure 13. Guidelines for the design of new candidates. 1. Introduction of negative groups in the proximity of K720; 2. Introduction of positive groups in the proximity of E897 and 3. Evaluation of new linkers which exploit the hydrophobicity of subpocket S2. Images were generated by MOE.[9]

Finally, in the absence of a ligand-cocrystal structure, a combined study of docking and molecular dynamics has been performed, affording new and relevant insights into the potential binding mode of our active ligands to the AF-2 site. These results also strongly support the main conclusions deduced from the SAR analysis and have provided enough information to hypothesize a bioactive conformation as a basis for the design of future new candidates.

EXPERIMENTAL SECTION

General Chemistry. Commercially available materials were obtained from Sigma−Aldrich and used without further purification. Deuterated solvents for NMR spectroscopy use were purchased from Apollo. Flash chromatography was carried out using standard silica gel 60 (230−400 mesh). Thin layer chromatography was performed using silica gel 60 TLC aluminum sheets with fluorescent indicator visualizing with UV light at 254 nm. NMR spectra were recorded on Bruker DPX-400 Avance spectrometers, operating at 400.13 and 600.1 MHz for ^{1}H NMR and 100.6 and 150.9 MHz for ^{13}C NMR. Shifts are referenced to the internal solvent signals.[38] NMR spectroscopic data were processed using MestReNova 6.0.2−5475 software. NMR data were processed using Bruker TOPSPIN software. HRMS spectra were measured on a Micromass LCT electrospray TOF instrument with a WATERS 2690 autosampler and methanol/acetonitrile as carrier solvent. Melting points were determined using a Stuart Scientific Melting Point SMP1 apparatus and are uncorrected. IR spectra were recorded either neat, as thin films on NaCl plates or as KBr discs (as specified) on a Perkin−Elmer Spectrum One FT-IR spectrometer. Compounds were prepared following the standard protocol depicted in Scheme 1.

*Synthesis of Methyl 2-naphthoate (**II**).* 2-Naphthoic acid (1.72 g, 10 mmol) was added to a solution of CH_3OH (20 mL) and HCl 37% (20 mL). The reaction mixture was heated at 90 °C, and the esterification was monitored by TLC until

dx.doi.org/10.1021/ci400189m | J. Chem. Inf. Model. 2013, 53, 2116−2130

complete consumption of the starting material was observed. Solvent was then removed *in vacuo*, and the reaction mixture was diluted with CH_2Cl_2 (30 mL) and washed with H_2O and saturated aqueous $NaHCO_3$. The aqueous phase was extracted with CH_2Cl_2 (2 × 30 mL), and the combined organic layers were washed with H_2O, dried over anhydrous Na_2SO_4, filtered, and concentrated *in vacuo* to give the crude product. The crude mixture was purified by flash column chromatography over silica gel (eluent CH_2Cl_2). Recrystallization from CH_3OH afforded pure product as a colorless solid (64%, MP: 76−79 °C); IR (neat) υ_{max}: 1679, 1594, 1542 cm^{-1}; ^1H NMR (400 MHz, DMSO-d6): δ 3.78 (s, 3H, *CH*$_3$), 7.36−7.42 (m, 2H, *Ar*), 7.73 (s, 2H, *Ar*), 7.83−7.89 (m, 2H, *Ar*), 8.48 (s, 1H, *Ar*) ppm; ^{13}C NMR (100 MHz, DMSO-d6): δ 51.6 (*CH*$_3$), 124.4 (CH, *Ar*), 125.9 (CH, *Ar*), 126.1 (q, *Ar*), 127.3 (CH, *Ar*), 128.4 (CH, *Ar*), 129.5 (CH, *Ar*), 132.7 (q, *Ar*), 136.5 (q, *Ar*), 165.3 (q, C_{CO}) ppm; HRMS: $C_{12}H_{10}O_2$ [M^+] requires (*m*/*e*) 186.0681, found 186.0675. HPLC Purity: 95%.

*Synthesis of 2-Naphthohydrazide (**III**).* To a solution of methyl 2-naphthoate (150 mg, 0.8 mmol) in EtOH (2 mL) was added hydrazine hydrate (100 μL, 3.2 mmol). The reaction mixture was heated to 160 °C in a microwave reactor until complete precipitation of hydrazide occurred (60 min). Completion of the reaction was confirmed by TLC. The reaction mixture was allowed to cool to 20 °C, filtered, and washed with hexane to give 2-naphthohydrazide as a white powder (85%, MP: 147−152 °C); IR (neat) υ_{max}: 3557, 3475, 3437, 1668, 1536, 1512 cm^{-1}; ^1H NMR (400 MHz, DMSO-d6): δ 2.74 (s, 2H, *NH*$_2$), 7.33 (m, 2H, *J* 6.9, *Ar*), 7.56 (d, 2H, *J* 7.1 *Ar*), 7.79 (s, 1H, *Ar*), 8.11−8.17 (m, 2H, *Ar*), 8.56 (s, 1H, *NH*) ppm; ^{13}C NMR (100 MHz, DMSO-d6): δ 122.5 (CH, *Ar*), 124.5 (CH, *Ar*), 125.3 (CH, *Ar*), 126.4 (CH, *Ar*), 127.2 (CH, *Ar*), 128.3 (CH, *Ar*), 129.2 (CH, *Ar*), 132.8 (q, *Ar*), 134.2 (q, *Ar*), 135.0 (q, *Ar*), 163.5 (q, C_{CO}) ppm; HRMS: $C_{11}H_{10}N_2O$ [M^+] requires (*m*/*e*) 186.0793 found at 186.0787.

*Synthesis of (E)-N′-(5-Chloro-2-hydroxybenzylidene)-2-naphthohydrazide (**26**).* To a solution of 2-naphthohydrazide (1.40 g, 7.5 mmol) in EtOH (20 mL) was added 2-hydroxy-4-chlorobenzaldehyde (1.17 g, 7.5 mmol), and the reaction was heated to 120 °C. Progress was monitored by TLC until complete consumption of the starting material was observed (6 h). The reaction mixture was allowed to cool to 20 °C and filtered, and the product was washed with hexane to give compound **26** as a brown powder (15%, MP: 260−262 °C); IR (neat) υ_{max}: 3593, 3496, 3362, 3384, 1665, 1658, 1625, 1688, 1477, 1432 cm^{-1}; ^1H NMR (400 MHz, DMSO-d6): δ 6.88 (d, 1H, J 8.5, *Ar*), 7.23 (d, 2H, J 8.5, *Ar*), 7.56 (s, 2H, *Ar*), 7.94 (d, 2H, J 7.5, *Ar*), 8.50 (s, 1H, *Ar*), 8.60 (s, 1H, *Ar*), 11.23 (s, 1H, *OH*), 12.30 (s, 1H, *NH*) ppm; ^{13}C NMR (100 MHz, DMSO-d6): δ 118.2 (CH, *Ar*), 120.7 (C), 122.9 (CH, *Ar*), 124.2 (CH, *Ar*), 127.0 (CH, *Ar*), 127.5 (CH, *Ar*), 127.7 (CH, *Ar*), 128.0 (CH, *Ar*), 128.2 (2 × CH, *Ar*), 128.9 (CH, *Ar*), 130.0 (CH, *Ar*), 130.8 (CH, *Ar*), 132.0 (q, *Ar*), 134.4 (q, *Ar*), 145.6 (CH, *Ar*), 156.0 (q, C_{CO}), 163.0 (q, C_{CO}) ppm; HRMS: $C_{18}H_{12}{}^{35}ClN_2O_2$ $[M-H]^-$ requires (*m*/*e*) 323.0587, found 323.065; HPLC purity: 96%.

*Synthesis of Methyl 3-hydroxy-2-naphthoate (**II**).* 3-Hydroxy-2-naphthoic acid (3.76 g, 20 mmol) was added to a solution of CH_3OH (20 mL) and HCl 37% (20 mL). The reaction mixture was heated at 90 °C, and the esterification was monitored by TLC until complete consumption of the starting material was observed. Solvent was then removed *in vacuo*, and the reaction mixture was diluted with CH_2Cl_2 (30 mL) and washed with H_2O and saturated aqueous $NaHCO_3$. The aqueous phase was extracted with CH_2Cl_2 (2 × 30 mL), and the combined organic layers were washed with H_2O, dried over anhydrous Na_2SO_4, filtered, and concentrated *in vacuo* to give the crude product. The crude mixture was purified by flash column chromatography over silica gel (eluent CH_2Cl_2−CH_3OH, 9:1) to afford the product as a colorless solid, which was recrystallized from EtOH (65%, MP: 74−76 °C); IR (neat) υ_{max}: 3563, 1649, 1584, 1533 cm^{-1}; ^1H NMR (400 MHz, DMSO-d6): δ 3.47 (s, 3H, *CH*$_3$), 7.24−7.31 (m, 2H, *Ar*), 7.69 (s, 2H, *Ar*), 7.94 (d, 2H, J 7.2, *Ar*), 8.21 (s, 1H, *OH*) ppm; ^{13}C NMR (100 MHz, DMSO-d6): δ 47.8 (*CH*$_3$), 110.3 (CH, *Ar*), 112.5 (q, *Ar*), 121.9 (CH, *Ar*), 126.8 (CH, *Ar*), 128.8 (q, *Ar*), 129.2 (CH, *Ar*), 129.8 (CH, *Ar*), 131.9 (CH, *Ar*), 132.0 (q, *Ar*), 157.8 (q, *Ar*), 164.6 (q, C_{CO}) ppm; HRMS: $C_{12}H_{10}NaO_3$ [M^++Na] requires (*m*/*e*) 225.0528, found 225.0521.

*Synthesis of 3-Hydroxy-2-naphthohydrazide (**III**).* To a solution of methyl 3-hydroxy-2-naphthoate (2.02 g, 10 mmol) in EtOH (10 mL) was added hydrazine hydrate (1,245 μL, 40 mmol). The reaction mixture was heated to 120 °C until complete precipitation of hydrazide occurred (15 min). Completion of the reaction was confirmed by TLC. The reaction mixture was allowed to cool to 20 °C, filtered, and washed with hexane to give the product as a beige powder, which was recrystallized from EtOH (99%, MP: 201−203 °C); IR (neat) υ_{max}: 3591, 3485, 3383, 1651, 1567, 1506 cm^{-1}; ^1H NMR (400 MHz, DMSO-d6): δ 2.16 (s, 1H, *NH*$_2$), 7.16 (d, 2H, J 7.2, *Ar*), 7.21−7.26 (m, 2H, *Ar*), 7.84 (s, 1H, *Ar*), 7.96 (s, 1H, *Ar*), 8.15 (s, 1H, *OH*), 8.56 (s, 1H, *NH*) ppm; ^{13}C NMR (100 MHz, DMSO-d6): δ 106.4 (CH, *Ar*), 114.2 (CH, *Ar*), 122.7 (q, *Ar*), 125.7 (CH, *Ar*), 126.8 (CH, *Ar*), 129.4 (CH, *Ar*), 130.4 (q, *Ar*), 133.7 (q, *Ar*), 156.4 (q, *Ar*), 161.3 (q, C_{CO}) ppm; HRMS: $C_{11}H_{10}N_2NaO_2$ [M^++Na] requires (*m*/*e*) 225.0640, found 225.0629.

*General Method for the Synthesis of Diarylhydrazides **27**−**45**.* To a solution of 3-hydroxy-2-naphthohydrazide (1.53 g, 7.5 mmol) in EtOH (20 mL) was added the appropriate aryl aldehyde or aryl ketone (7.5 mmol). The reaction mixture was heated to 120 °C and monitored by TLC until complete consumption of the starting material was observed (6 h). The reaction mixture was allowed to cool to 20 °C and filtered, and the products were washed with hexane to give products as powders, which were purified further by recrystallization from EtOH.

*(E)-N′-Benzylidene-3-hydroxy-2-naphthohydrazide (**27**).* Beige powder (85%, MP: 227−230 °C[39]); IR (neat) υ_{max}: 3453, 3242, 3047, 1626, 1631, 1613, 1561 cm^{-1}; ^1H NMR (400 MHz, DMSO-d6): δ 7.34 (s, 1H, *Ar*), 7.38 (dd, J 8.2, 7.3, 1H, *Ar*), 7.49 (ddd, J 6.6, *Ar*), 7.50 (dd, J 7.5, 1H, *Ar*), 7.53 (dd, J 7.3, 7.3, 1H, *Ar*), 7.78 (d, J 7.2, 1H, *Ar*), 7.79 (d, J 7.2, 1H, *Ar*), 7.93 (d, J 8.2, 1H, *Ar*), 8.47 (s, 1H, *Ar*), 8.48 (s, 1H, H_{CN}), 11.30 (s, 1H, *NH*), 11.99 (s, 1H, *OH*) ppm; ^{13}C NMR (100 MHz, DMSO-d6): δ 110.6 (CH, *Ar*), 120.4 (q, *Ar*), 123.9 (CH, *Ar*), 125.7 (CH, *Ar*), 126.8 (q, *Ar*), 127.3 (CH, *Ar*), 128.3 (CH, *Ar*), 128.7 (CH, *Ar*), 128.9 (CH, *Ar*), 130.2 (CH, *Ar*), 130.3 (CH, *Ar*), 134.1 (q, *Ar*), 135.8 (q, *Ar*), 148.5 (CH, C_{CN}), 154.1 (q, *Ar*), 163.8 (q, C_{CO}) ppm; HRMS: $C_{18}H_{15}N_2O_2$ [M^++H] requires (*m*/*e*) 291.1134, found 291.1141; HPLC purity: 100%.

*(E)-3-Hydroxy-N′-(2-hydroxybenzylidene)-2-naphthohydrazide (**28**).* Yellow powder (90%, MP: 217−219 °C[40]); IR (neat) υ_{max}: 3478, 3352, 3256, 1660, 1646, 1632, 1596, 1567 cm^{-1}; ^1H NMR (400 MHz, DMSO-d6): δ 5.63 (s, 1H, *OH*), 6.93−6.98 (m, 2H, *Ar*), 7.31−7.40 (m, 3H, *Ar*), 7.52 (t, 1H, J

dx.doi.org/10.1021/ci400189m | J. Chem. Inf. Model. 2013, 53, 2116−2130

7.52, *Ar*), 7.58 (d, 1H, J 6.5, *Ar*), 7.77 (d, 1H, J 8.5, *Ar*), 7.91 (d, 1H, J 8.0, *Ar*), 8.47 (s, 1H, *Ar*), 8.69 (s, 1H, H_{CN}), 11.22 (s, 1H, *OH*), 12.17 (s, 1H, *NH*) ppm; ^{13}C NMR (400 MHz, DMSO-d6): δ 110.6 (CH, *Ar*), 116.5 (CH, *Ar*), 118.7 (q, *Ar*), 119.4 (CH, *Ar*), 120.1 (CH, *Ar*), 123.9 (q, *Ar*), 125.9 (CH, *Ar*), 126.8 (q, *Ar*), 128.3 (CH, *Ar*), 128.7 (CH, *Ar*), 129.4 (q, *Ar*), 130.3 (CH, *Ar*), 131.6 (CH, *Ar*), 135.9 (q, *Ar*), 148.7 (CH, C_{CN}), 154.0 (q, *Ar*), 157.5 (q, *Ar*), 163.6 (q, C_{CO}) ppm; HRMS: $C_{18}H_{14}N_2NaO_3$ [M$^+$+Na] requires (*m*/*e*) 329.0902, found 329.0903; HPLC Purity: 97%.

*(E)-3-Hydroxy-N′-(2-hydroxy-5-methylbenzylidene)-2-naphthohydrazide (**29**).* Beige powder (89%, MP: 254−258 °C); IR (neat) υ_{max}: 3542, 3388, 3277, 1669, 1657, 1631 cm^{-1}; ^{1}H NMR (400 MHz, DMSO-d6): δ 2.27 (s, 3H, CH_3), 6.86 (d, 1H, J 8.5, *Ar*), 7.19 (dd, 1H, J 1.8, 1.7, *Ar*), 7.35−7.40 (m, 3H, *Ar*), 7.51−7.55 (m, 1H, *Ar*), 7.77 (d, 1H, J 8.0, *Ar*), 7.92 (d, 1H, J 8.0, *Ar*), 8.47 (s, 1H, H_{CN}), 8.65 (s, 1H, *Ar*), 10.97 (s, 1H, *NH*), 11.31 (s, 1H, *OH*), 12.17 (s, 1H, *OH*) ppm; ^{13}C NMR (400 MHz, DMSO-d6): δ 20.4 (CH_3), 111.1 (CH, *Ar*), 116.8 (CH, *Ar*), 118.8 (q, *Ar*), 120.5 (CH, *Ar*), 124.3 (q, *Ar*), 126.3 (CH, *Ar*), 127.2 (q, *Ar*), 128.4 (CH, *Ar*), 128.8 (q, *Ar*), 129.1 (CH, *Ar*), 129.7 (q, *Ar*), 130.8 (CH, *Ar*), 132.8 (CH, *Ar*), 136.4 (q, *Ar*), 149.1 (q, C_{CN}), 154.6 (q, *Ar*), 155.8 (q, *Ar*), 164.1 (q, C_{CO}) ppm; HRMS: $C_{19}H_{16}N_2O_3$ [M$^+$] requires (*m*/*e*) 320.1161, found 320.0930; HPLC Purity: 100%.

*(E)-N′-(5-(tert-Butyl)-2-hydroxybenzylidene)-3-hydroxy-2-naphthohydrazide (**30**).* Beige powder (83%, MP: 247−250 °C); IR (neat) υ_{max}: 3411.8, 3321.9, 3164.3, 1636.8, 1632.9, 1626.4, 1567.5 cm^{-1}; ^{1}H NMR (400 MHz, DMSO-d6): δ 1.15 (s, 9H, 3 × CH_3), 6.90 (d, 1H, J 8.5, *Ar*), 7.35−7.41 (m, 2H, *Ar*), 7.53 (t, 2H, J 7.3, *Ar*), 7.77 (s, 1H, *Ar*), 7.92 (s, 1H, *Ar*), 8.17 (s, 1H, *Ar*), 8.49 (s, 1H, *Ar*), 8.63 (s, 1H, *NH*), 11.30 (s, 1H, *OH*), 12.15 (s, 1H, *OH*) ppm; ^{13}C NMR (400 MHz, DMSO-d6): δ 31.7 (3 × CH_3), 34.3 (q, *C*), 111.0 (CH, *Ar*), 116.6 (CH, *Ar*), 118.4 (q, *Ar*), 120.6 (CH, *Ar*), 124.3 (CH, *Ar*), 126.0 (q, *Ar*), 126.3 (CH, *Ar*), 127.2 (CH, *Ar*), 128.8 (CH, *Ar*), 129.2 (CH, *Ar*), 129.4 (CH, *Ar*), 130.8 (CH, *Ar*), 136.4 (q, *Ar*), 142.0 (q, *Ar*), 149.6 (CH, C_{CN}), 154.5 (q, *Ar*), 155.8 (q, *Ar*), 164.0 (q, C_{CO}) ppm; HRMS: $C_{22}H_{21}N_2O_3$ [M$^-$−H] requires (*m*/*e*) 361.1550, found 361.1556; HPLC Purity: 100%.

*(E)-N′-(2,5-Dihydroxybenzylidene)-3-hydroxy-2-naphthohydrazide (**31**).* Yellow powder (89%, MP: 232−236 °C); IR (neat) υ_{max}: 3585, 3561, 3490, 3357, 3148, 1646, 1653, 1639, 1545 cm^{-1}; ^{1}H NMR (400 MHz, DMSO-d6): δ 6.77 (t, 2H, J 2.5, *Ar*), 7.03 (s, 1H, *Ar*), 7.34−7.41 (m, 2H, *Ar*), 7.53 (d, 1H, J 7.0, *Ar*), 7.77 (d, 1H, J 8.2, *Ar*), 7.91 (d, 1H, J 8.0, *Ar*), 8.48 (s, 1H, *Ar*), 8.62 (s, 1H, *Ar*), 9.04 (s, 1H, *NH*), 10.34 (s, 1H, *OH*), 11.33 (s, 1H, *OH*), 12.10 (s, 1H, *OH*) ppm; ^{13}C NMR (400 MHz, DMSO-d6): δ 111.1 (CH, *Ar*), 114.1 (CH, *Ar*), 117.6 (CH, *Ar*), 119.5 (CH, *Ar*), 119.7 (q, *Ar*), 120.4 (CH, *Ar*), 124.3 (CH, *Ar*), 126.3 (CH, *Ar*), 127.2 (CH, *Ar*), 128.8 (CH, *Ar*), 129.1 (CH, *Ar*), 130.7 (q, *Ar*), 136.4 (q, *Ar*), 148.6 (CH, C_{CN}), 150.4 (q, *Ar*), 150.8 (q, *Ar*), 154.7 (q, *Ar*), 164.1 (q, C_{CO}) ppm; HRMS: $C_{18}H_{13}N_2O_4$ [M$^-$−H] requires (*m*/*e*) 321.0875, found 321.0865; HPLC Purity: 100%.

*(E)-3-Hydroxy-N′-(2-hydroxy-5-methoxybenzylidene)-2-naphthohydrazide (**32**).* White powder (95%, MP: 287−292 °C); IR (neat) υ_{max}: 3529, 3489, 3357, 3250, 1649, 1636, 1620, 1550, 1453 cm^{-1}; ^{1}H NMR (400 MHz, DMSO-d6): δ 3.75 (s, 3H, CH_3), 6.91−6.99 (m, 2H, *Ar*), 7.17 (d, 1H, J 2.8, *Ar*), 7.34−7.41 (m, 2H, *Ar*), 7.51 (td, 2H, J 13.8, 8.3, 1.3, *Ar*), 7.77 (d, 1H, *J* 8.3, *Ar*), 7.91 (d, 1H, J 8.2, *Ar*), 8.47 (s, 1H, *OH*), 8.67 (s, 1H, *OH*) ppm; ^{13}C NMR (400 MHz, DMSO-d6): δ 56.0 (CH_3), 111.0 (CH, *Ar*), 112.5 (CH, *Ar*), 117.8 (CH, *Ar*), 119.0 (CH, *Ar*), 119.4 (CH, *Ar*), 120.6 (CH, *Ar*), 124.3 (q, *Ar*), 126.3 (CH, *Ar*), 127.2 (CH, *Ar*), 128.8 (CH, *Ar*), 129.1 (CH, *Ar*), 130.7 (q, *Ar*), 136.4 (q, *Ar*), 148.5 (CH, C_{CN}), 152.0 (q, *Ar*), 152.6 (q, *Ar*), 154.6 (q, *Ar*), 164.1 (q, C_{CO}) ppm; HRMS: $C_{19}H_{15}N_2O_4$ [M$^-$−H] requires (*m*/*e*) 335.1032, found 335.1045; HPLC Purity: 95%.

*(E)-4-Hydroxy-3-((2-(3-hydroxy-2-naphthoyl)hydrazono)-methyl)benzoic Acid (**33**).* White powder identified as X (85%, MP: 332−334 °C); IR (neat) υ_{max}: 3252, 2982, 1671, 1637, 1609, 1552, 1524, 1492, 1450, 1361, 1346, 1295, 1274, 1232, 1177, 1149, 1129, 1074, 955, 918, 888, 872, 842, 792, 769, 742, 731, 690, 671 cm^{-1}; ^{1}H NMR (400 MHz, DMSO-d6): δ 12.77 (s, 1H, *OH*), 12.23 (s, 1H, *OH*), 11.78 (s, 1H, *NH*), 11.29 (s, 1H, CO_2H), 8.75 (s, 1H, H_{CN}), 8.48 (s, 1H, *Ar*), 8.30 (d, 1H, J 1.9, *Ar*), 7.95−7.88 (m, 2H, *Ar*), 7.79 (d, 1H, J 8.3, *Ar*), 7.53 (app. t, J 7.6, 7.4, *Ar*), 7.38 (app. t, 1H, J 7.6, *Ar*), 7.35 (s, 1H, *Ar*), 7.05 (d, 1H, J 8.6, *Ar*) ppm; ^{13}C NMR (100 MHz, DMSO-d6): δ 111.0 (CH, *Ar*), 117.0 (CH, *Ar*), 119.5 (q, *Ar*), 120.6 (q, *Ar*), 122.5 (q, *Ar*), 124.3 (CH, *Ar*), 126.3 (CH, *Ar*), 127.2 (q, *Ar*), 128.8 (CH, *Ar*), 129.2 (CH, *Ar*), 130.8 (CH, *Ar*), 130.9 (CH, *Ar*), 133.1 (CH, *Ar*), 136.4 (q, *Ar*), 147.4 (CH, C_{CN}), 154.5 (q, *Ar*), 161.4 (q, *Ar*), 164.2 (q, C_{CO}), 167.2 (q, C_{CO}) ppm; HRMS: $C_{19}H_{13}N_2O_5$ [M$^-$−H] requires (*m*/*e*) 349.0824, found 349.0831; HPLC Purity: 95%.

*(E)-Methyl 4-Hydroxy-3-((2-(3-hydroxy-2-naphthoyl)-hydrazono)methyl)benzoate (**34**).* White powder (83%, MP: 290−292 °C); IR (neat) υ_{max}: 3223, 1729, 1646, 1555, 1441, 1401, 1376, 1358, 1301, 1276, 1226, 1106, 1072, 972, 953, 868, 798, 763, 741, 728 cm^{-1}; ^{1}H NMR (400 MHz, DMSO-d6): δ 3.85 (s, 3H, CH_3), 7.05 (d, 1H, J 8.6, *Ar*), 7.33 (s, 1H, *Ar*), 7.37 (app. t, 1 H, J 7.7, 7.3, *Ar*), 7.52 (app. t, 1H, J 7.7, 7.3, *Ar*), 7.77 (d, 1H, J 8.3, *Ar*), 7.91 (td, 2H, J 8.6, 1.9, *Ar*), 8.32 (d, 1H, J 2.1, *Ar*), 8.46 (s, 1H, *Ar*), 8.74 (s, 1H, H_{CN}), 11.27 (s, 1H, *OH*), 11.79 (s, 1H, *NH*), 12.21 (s, 1H, *OH*) ppm; ^{13}C NMR (100 MHz, DMSO-d6): δ 52.4 (CH_3), 111.0 (CH, *Ar*), 117.2 (CH, *Ar*), 119.8 (q, *Ar*), 120.6 (q, *Ar*), 121.3 (q, *Ar*), 124.3 (CH, *Ar*), 126.3 (CH, *Ar*), 127.2 (q, *Ar*), 128.8 (CH, *Ar*), 129.1 (CH, *Ar*), 130.4 (CH, *Ar*), 130.8 (CH, *Ar*), 132.9 (CH, *Ar*), 136.4 (q, *Ar*), 146.9 (CH, C_{CN}), 154.5 (q, *Ar*), 161.7 (q, *Ar*), 164.2 (q, C_{CO}), 166.2 (q, C_{CO}), ppm; HRMS: $C_{20}H_{15}N_2O_5$ [M$^-$−H] requires (*m*/*e*) 363.0981, found 363.0978; HPLC Purity: 95%.

*(E)-3-Hydroxy-N′-(2-hydroxy-5-iodobenzylidene)-2-naphthohydrazide (**35**).* White powder (96%, MP: 281−288 °C); IR (neat) υ_{max}: 3564, 3483, 3360, 3148, 1671, 1643, 1621 cm^{-1}; ^{1}H NMR (400 MHz, DMSO-d6): δ 6.80 (d, 1H, J 8.5, *Ar*), 7.34−7.40 (m, 2H, *Ar*), 7.52 (s, 1H, *Ar*), 7.58 (dd, 1H, J 8.5, 2.3, *Ar*), 7.77 (d, 1H, J 8.3, *Ar*), 7.91 (d, 1H, J 8.3, *Ar*), 7.97 (d, 1H, J 2.2, *Ar*), 8.46 (s, 1H, *Ar*), 8.62 (s, 1H, H_{CN}), 11.23 (s, 1H, *NH*), 12.22 (s, 1H, *OH*) ppm. ^{13}C NMR (400 MHz, DMSO-d6): δ 81.9 (q, *Ar*), 111.0 (CH, *Ar*), 119.6 (CH, *Ar*), 120.6 (q, *Ar*), 122.3 (CH, *Ar*), 124.3 (q, *Ar*), 126.3 (CH, *Ar*), 127.2 (CH, *Ar*), 128.8 (CH, *Ar*), 129.1 (CH, *Ar*), 130.8 (q, *Ar*), 136.4 (CH, *Ar*), 136.7 (CH, *Ar*), 140.0 (CH, *Ar*), 146.5 (CH, C_{CN}), 154.5 (q, *Ar*), 157.5 (q, *Ar*), 164.2 (q, C_{CO}) ppm; HRMS: $C_{18}H_{12}{}^{127}IN_2O_3$ [M$^-$−H] requires (*m*/*e*) 430.9893, found 430.9934; HPLC Purity: 100%.

*(E)-3-Hydroxy-N′-(2-hydroxy-5-nitrobenzylidene)-2-naphthohydrazide (**36**).* Yellow powder (95%, MP: 258−260 °C); IR (neat) υ_{max}: 3435, 3353, 3142, 1694, 1650, 1626, 1540 cm^{-1}; ^{1}H NMR (400 MHz, DMSO-d6): δ 7.13 (d, 1H, J 9.0, *Ar*), 7.34−7.40 (m, 2H, *Ar*), 7.50 (td, 1H, J 14.0, 8.0, 1.0, *Ar*), 7.77 (d, 1H, J 8.3, *Ar*), 7.91 (d, 1H, J 8.2, *Ar*), 8.18 (dd, 1H, J 12.0,

3.0, *Ar*), 8.46 (s, 1H, *Ar*), 8.61 (d, 1H, J 2.8, *Ar*), 8.76 (s, 1H, H_{CN}), 12.29 (s, 2H, *OH*) ppm; ^{13}C NMR (400 MHz, DMSO-d6): δ 111.0 (CH, *Ar*), 117.6 (CH, *Ar*), 120.4 (q, *Ar*), 120.7 (CH, *Ar*), 124.2 (CH, *Ar*), 124.3 (CH, *Ar*), 126.3 (CH, *Ar*), 127.2 (2 × CH, *Ar*), 128.8 (CH, *Ar*), 129.1 (CH, *Ar*), 130.9 (q, *Ar*), 136.4 (q, *Ar*), 140.4 (q, *Ar*), 145.3 (CH, C_{CN}), 154.4 (q, *Ar*), 163.1 (q, *Ar*), 164.3 (q, C_{CO}) ppm; HRMS: $C_{18}H_{12}N_3O_5$ [M$^-$−H] requires (*m*/*e*) 350.0777, found 350.0786; HPLC Purity: 95%.

*(E)-3-Hydroxy-N′-(2-hydroxy-3-methylbenzylidene)-2-naphthohydrazide (**37**).* White powder (88%, MP: 278−285 °C); IR (neat) υ_{max}: 3538, 3451, 3385, 3295, 1649, 1629, 1616, 1584 cm^{-1}; ^{1}H NMR (400 MHz, DMSO-d6): δ 2.24 (s, 3H, *CH3*), 6.88 (t, 1H, J 7.5, *Ar*), 7.23 (d, 1H, J 7.3, *Ar*), 7.30 (d, 1H, J 1.0, *Ar*), 7.36−7.41 (m, 2H, *Ar*), 7.51−7.58 (m, 1H, *Ar*), 7.78 (d, 1H, J 8.2, *Ar*), 7.93 (d, 1H, J 8.0, *Ar*), 8.48 (s, 1H, *Ar*), 8.64 (s, 1H, H_{CN}), 11.26 (s, 1H, *OH*), 11.90 (s, 1H, *OH*), 12.23 (s, 1H, *NH*) ppm; ^{13}C NMR (400 MHz, DMSO-d6): δ 15.9 (CH_3), 111.1 (CH, *Ar*), 117.6 (q, *Ar*), 119.4 (CH, *Ar*), 120.6 (CH, *Ar*), 124.3 (CH, *Ar*), 125.5 (q, *Ar*), 126.3 (q, *Ar*), 127.3 (CH, *Ar*), 128.8 (CH, *Ar*), 129.2 (CH, *Ar*), 129.3 (CH, *Ar*), 131.0 (q, *Ar*), 133.1 (CH, *Ar*), 136.4 (q, *Ar*), 151.1 (CH, C_{CN}), 154.3 (q, *Ar*), 156.5 (q, *Ar*), 163.8 (q, C_{CO}) ppm; HRMS: $C_{19}H_{15}N_2O_3$ [M$^-$−H] requires (*m*/*e*) 319.1083, found 319.1081; HPLC Purity: 97%.

*(E)-3-Hydroxy-N′-(2-hydroxy-3-methoxybenzylidene)-2-naphthohydrazide (**38**).* Beige powder (85%, MP: 288−291 °C[41]); IR (neat) υ_{max}: 3468, 3372, 3284, 1647, 1631, 1609, 1586, 1568 cm^{-1}; ^{1}H NMR (400 MHz, DMSO-d6): δ 3.84 (s, 3H, CH_3), 6.87 (t, 1H, J 7.9, *Ar*), 7.05 (dd, 1H, J 6.8, 1.2, *Ar*), 7.19 (dd, 1H, J 6.8, 1.3, *Ar*), 7.34−7.41 (m, 2H, *Ar*), 7.51−7.60 (m, 1H, *Ar*), 7.77 (d, 1H, J 8.3, *Ar*), 7.91 (d, 1H, J 8.0, *Ar*), 8.47 (s, 1H, *Ar*), 8.71 (s, 1H, H_{CN}), 10.90 (s, 1H, *OH*), 11.29 (s, 1H, *OH*), 12.15 (s, 1H, *NH*) ppm; ^{13}C NMR (400 MHz, DMSO-d6): δ 59.4 (s, 1H, CH_3), 111.1 (CH, *Ar*), 114.4 (CH, *Ar*), 119.4 (CH, *Ar*), 119.6 (CH, *Ar*), 120.5 (CH, *Ar*), 121.2 (q, *Ar*), 124.3 (CH, *Ar*), 126.3 (CH, *Ar*), 127.2 (CH, *Ar*), 128.8 (CH, *Ar*), 129.1 (CH, *Ar*), 130.8 (q, *Ar*), 136.4 (q, *Ar*), 147.7 (CH, C_{CN}), 148.5 (q, *Ar*), 149.1 (q, *Ar*), 154.6 (q, *Ar*), 1641 (q, C_{CO}) ppm; HRMS: $C_{19}H_{15}N_2O_4$ [M$^-$−H] requires (*m*/*e*) 335.1032, found 335.1028; HPLC Purity: 95%.

*(E)-N′-(3-Chloro-2-hydroxybenzylidene)-3-hydroxy-2-naphthohydrazide (**39**).* Beige powder (92%, MP: 238−244 °C); IR (neat) υ_{max}: 3538, 3517, 3347, 3258, 1663, 1629, 1621, 1568, 1440 cm^{-1}; ^{1}H NMR (400 MHz, DMSO-d6): δ 6.97 (t, 1H, J 7.8, *Ar*), 7.26−7.36 (m, 2H, *Ar*), 7.507.56 (m, 3H, *Ar*), 7.78 (d, 1H, J 8.3, *Ar*), 7.93 (d, 1H, J 8.0, *Ar*), 8.47 (s, 1H, H_{CN}), 8.68 (s, 1H, *Ar*), 9.11 (s, 1H, *OH*) 11.20 (s, 1H, *OH*), 12.40 (s, 1H, *NH*) ppm; ^{13}C NMR (400 MHz, DMSO-d6): δ 111.2 (CH, *Ar*), 120.1 (q, *Ar*), 120.6 (CH, *Ar*), 120.7 (q, *Ar*), 120.9 (CH, *Ar*), 124.4 (CH, *Ar*), 126.4 (CH, *Ar*), 127.3 (CH, *Ar*), 128.8 (CH, *Ar*), 129.2 (CH, *Ar*), 130.0 (CH, *Ar*), 131.2 (CH, *Ar*), 132.0 (q, *Ar*), 136.4 (q, *Ar*), 149.6 (CH, C_{CN}), 153.8 (q, *Ar*), 154.1 (q, *Ar*), 163.8 (q, C_{CO}) ppm; HRMS: $C_{18}H_{12}{}^{35}ClN_2O_3$ [M$^-$−H] requires (*m*/*e*) 339.0536, found 339.0543; HPLC Purity: 100%.

*(E)-N′-(5-Chloro-2-hydroxy-3-methoxybenzylidene)-3-hydroxy-2-naphthohydrazide (**40**).* Yellow powder (98%, MP: 298−300 °C); IR (neat) υ_{max}: 3515, 3493, 3275, 3127, 1656, 1647, 1615, 631 cm^{-1}; ^{1}H NMR (400 MHz, DMSO-d6): δ 3.86 (s, 3H, CH_3), 7.10 (d, 1H, J 2.5, *Ar*), 7.29−7.34 (m, 3H, *Ar*), 7.52 (d, 1H, J 7.5, *Ar*), 7.76 (d, 1H, J 8.5, *Ar*), 7.90 (d, 1H, J 8.5, *Ar*), 8.45 (s, 1H, *Ar*), 8.66 (s, 1H, H_{CN}), 10.84 (s, 1H, *OH*), 11.24 (s, 1H, *OH*), 12.20 (s, 1H, *NH*) ppm; ^{13}C NMR (400 MHz, DMSO-d6): δ 56.3 (CH_3), 110.5 (CH, *Ar*), 113.5 (CH, *Ar*), 118.6 (q, *Ar*), 120.1 (CH, *Ar*), 120.2 (CH, *Ar*), 122.8 (CH, *Ar*), 123.8 (q, *Ar*), 125.9 (CH, *Ar*), 126.8 (q, *Ar*), 128.3 (CH, *Ar*), 128.7 (CH, *Ar*), 130.3 (q, *Ar*), 135.9 (q, *Ar*), 145.9 (q, *Ar*), 146.3 (q, C_{CN}), 149.0 (q, *Ar*), 154.0 (q, *Ar*), 163.7 (q, C_{CO}) ppm; HRMS: $C_{19}H_{14}{}^{35}ClN_2O_4$ [M$^-$−H] requires (*m*/*e*) 369.0642, found 369.0721; HPLC Purity: 100%.

*(E)-3-Hydroxy-N′-(2-methoxybenzylidene)-2-naphthohydrazide (**41**).* Beige powder (81%, MP: 274−279 °C); IR (neat) υ_{max}: 3436, 3357, 3240, 1640, 1630, 1619, 1537 cm^{-1}; ^{1}H NMR (400 MHz, DMSO-d6): δ 3.89 (s, 3H, CH_3), 7.04 (t, 1H, J 7.5, *Ar*), 7.13 (d, 1H, J 8.3, *Ar*), 7.33 (s, 1H, *Ar*), 7.36−7.40 (m, 1H, *Ar*), 7.44−7.49 (m, 1H, *Ar*), 7.50−7.59 (m, 1H, *Ar*), 7.77 (d, 1H, J 8.3, *Ar*), 7.90 (m, 1H, *Ar*), 8.49 (s, 1H, *Ar*), 8.82 (s, 1H, *Ar*), 11.40 (s, 1H, H_{CN}), 12.07 (s, 1H, *OH*) ppm; ^{13}C NMR (400 MHz, DMSO-d6): δ 56.2 (CH_3), 111.1 (CH, *Ar*), 112.4 (CH, *Ar*), 120.2 (q, *Ar*), 121.3 (CH, *Ar*), 122.5 (CH, *Ar*), 124.3 (CH, *Ar*), 126.1 (CH, *Ar*), 126.3 (CH, *Ar*), 127.2 (CH, *Ar*), 128.8 (CH, *Ar*), 129.1 (CH, *Ar*), 130.3 (q, *Ar*), 132.4 (CH, *Ar*), 136.4 (q, *Ar*), 144.6 (CH, C_{CN}), 155.1 (q, *Ar*), 158.4 (q, *Ar*), 164.7 (q, C_{CO}) ppm; HRMS: $C_{19}H_{15}N_2O_3$ [M$^-$−H] requires (*m*/*e*) 319.1083, found 319.1087; HPLC Purity: 96%.

*(E)-N′-(5-Bromo-2-methoxybenzylidene)-3-hydroxy-2-naphthohydrazide (**42**).* Yellow powder (83%, MP: 293−297 °C); IR (neat) υ_{max}: 3583, 3453, 3369, 3176, 1691, 1658, 1655, 1560 cm^{-1}; ^{1}H NMR (400 MHz, DMSO-d6): δ 3.89 (s, 3H, CH_3), 7.12 (d, 1H, J 9.0, *Ar*), 7.33 (s, 1H, *Ar*), 7.36 (d, 1H, J 7.0, *Ar*), 7.50−7.56 (m, 1H, *Ar*), 7.60 (d, 1H, J 2.5, *Ar*), 7.76 (d, 1H, J 8.0, *Ar*), 7.90 (d, 1H, J 8.0, *Ar*), 7.98 (d, 1H, J 2.5, *Ar*), 8.46 (s, 1H, *Ar*), 8.49 (s, 1H, H_{CN}), 8.73 (s, 1H, *Ar*), 11.29 (s, 1H, *OH*), 12.13 (s, 1H, *NH*) ppm; ^{13}C NMR (400 MHz, DMSO-d6): δ 56.6 (CH_3), 111.1 (CH, *Ar*), 113.0 (q, *Ar*), 115.0 (CH, *Ar*), 120.5 (q, *Ar*), 124.3 (CH, *Ar*), 124.8 (CH, *Ar*), 126.3 (CH, *Ar*), 127.2 (CH, *Ar*), 128.0 (CH, *Ar*), 128.8 (CH, *Ar*), 129.1 (CH, *Ar*), 130.5 (q, *Ar*), 134.4 (q, *Ar*), 136.4 (CH, *Ar*), 142.7 (CH, C_{CN}), 154.8 (q, *Ar*), 157.5 (q, *Ar*), 164.7 (q, C_{CO}) ppm; HRMS: $C_{19}H_{14}{}^{79}BrN_2O_3$ [M$^-$−H] requires (*m*/*e*) 397.0188, found 397.0243; HPLC Purity: 95%.

*(E)-N′-(2-Aminobenzylidene)-3-hydroxy-2-naphthohydrazide (**43**).* White powder (73%, MP: 262−264 °C); IR (neat) υ_{max}: 3414, 3305, 3254, 3053, 1596, 1551, 1512, 1485, 1446, 1395, 1363, 1318, 1272, 1218, 1159, 1074, 1013, 957, 934, 906, 875, 855, 793, 774, 757, 742, 676 cm^{-1}; ^{1}H NMR (400 MHz, DMSO-d6): δ 6.61 (app. t, J 7.4, 7.3, 1H, *Ar*), 6.78 (d, J 8.2, 1H, *Ar*), 7.10 (s, 2H, NH_2), 7.15 (app. t, J 7.5, 7.4, 1H, *Ar*), 7.23 (d, J 7.6, 1H, *Ar*), 7.35 (s, 1H, *Ar*), 7.38 (app. t, J 7.5, 1H, *Ar*), 7.53 (app. t, J 7.7, 7.2, 1H, *Ar*), 7.78 (d, J 8.3, 1H, *Ar*), 7.93 (d, J 8.2, 1H, *Ar*), 8.49 (s, 1H, *Ar*), 8.53 (s, 1H, H_{CN}), 11.44 (s, 1H, *NH*), 11.96 (s, 1H, *OH*), ppm; ^{13}C NMR (100 MHz, DMSO-d6): δ 111.1 (CH, *Ar*), 115.0 (q, *Ar*), 115.4 (CH, *Ar*), 115.6 (CH, *Ar*), 120.3 (q, *Ar*), 124.3 (CH, *Ar*), 126.3 (CH, *Ar*), 127.2 (q, *Ar*), 128.7 (CH, *Ar*), 129.1 (CH, *Ar*), 130.5 (CH, *Ar*), 131.1 (CH, *Ar*), 132.9 (CH, *Ar*), 136.3 (q, *Ar*), 148.5 (q, *Ar*), 152.3 (CH, C_{CN}), 154.8 (q, *Ar*), 163.9 (q, C_{CO}) ppm; HRMS: $C_{18}H_{14}N_3O_2$ [M$^-$−H] requires (*m*/*e*) 304.1086, found 304.1090; HPLC Purity: 95%.

*(E)-3-Hydroxy-N′-(2-nitrobenzylidene)-2-naphthohydrazide (**44**).* White powder (15%, MP: 220−222 °C); IR (neat) υ_{max}: 3060, 2923, 2854, 1643, 1626, 1597, 1542, 1515, 1476, 1450, 1400, 1346, 1313, 1209, 1178, 1146, 1105, 1073, 949, 928, 905, 877, 859, 838, 785, 740, 691, 670 cm^{-1}; ^{1}H NMR (400 MHz, DMSO-d6): δ 7.34 (s, 1H, *Ar*), 7.38 (app. t, J 7.7,

dx.doi.org/10.1021/ci400189m | J. Chem. Inf. Model. 2013, 53, 2116−2130

7.3, 1H, *Ar*), 7.53 (app. t, J 7.6, 7.5, 1H, *Ar*), 7.73 (app. t, J 8.0, 7.6, 1H, *Ar*), 7.79 (d, J 8.4, 1H, *Ar*), 7.87 (app. t, J 7.6, 7.5, 1H, *Ar*), 7.94 (d, J 8.2, 1H, *Ar*), 8.12 (d, J 8.1, 1H, *Ar*), 8.17 (d, J 7.7, 1H, *Ar*), 8.44 (s, 1H, *Ar*), 8.87 (s, 1H, H_{CN}), 11.20 (s, 1H, *NH*), 12.32 (s, 1H, *OH*) ppm; ^{13}C NMR (100 MHz, DMSO-d6): δ 111.0 (CH, *Ar*), 121.0 (q, *Ar*), 124.3 (CH, *Ar*), 125.2 (CH, *Ar*), 126.3 (CH, *Ar*), 127.2 (q, *Ar*), 128.6 (CH, *Ar*), 128.8 (CH, *Ar*), 129.1 (q, *Ar*), 129.1 (CH, *Ar*), 130.7 (CH, *Ar*), 131.3 (CH, *Ar*), 134.3 (CH, *Ar*), 136.3 (q, *Ar*), 144.2 (CH, C_{CN}), 148.8 (q, *Ar*), 154.5 (q, *Ar*), 164.7 (q, C_{CO}) ppm; HRMS: $C_{18}H_{12}N_3O_4$ $[M-H]^-$ requires (*m*/*e*) 334.0828, found 334.0819; HPLC Purity: 95%.

*(E)-N′-(5-Chloro-2-nitrobenzylidene)-3-hydroxy-2-naphthohydrazide (**45**).* White powder (70%, MP: 252−254 °C); IR (neat) υ_{max}: 3414, 3305, 3254, 3053, 1596, 1551, 1512, 1485, 1446, 1395, 1363.08, 1318, 1272, 1218, 1159, 1074, 1013, 957, 934, 906, 875, 855, 793, 774, 757, 742, 676 cm^{-1}; ^{1}H NMR (400 MHz, DMSO-d6): δ 7.34 (s, 1H, *Ar*), 7.38 (app. t, J 7.5, 7.4, 1H, *Ar*), 7.53 (app. t, J 7.6, 7.4, 1H, *Ar*), 7.78 (d, J 8.6, 2H, *Ar*), 7.93 (d, J 8.2, 1H, *Ar*), 8.11 (d, J 2.0, 1H, *Ar*), 8.17 (d, J 8.8, 1H, *Ar*), 8.42 (s, 1H, *Ar*), 8.87 (s, 1H, H_{CN}), 11.14 (s, 1H, *NH*), 12.40 (s, 1H, *OH*) ppm; ^{13}C NMR (100 MHz, DMSO-d6): δ 111.0 (CH, *Ar*), 121.2 (q, *Ar*), 124.3 (CH, *Ar*), 126.3 (CH, *Ar*), 127.2 (q, *Ar*), 127.5 (CH, *Ar*), 127.7 (CH, *Ar*), 128.8 (CH, *Ar*), 129.1 (CH, *Ar*), 130.8 (CH, *Ar*), 130.9 (CH, *Ar*), 131.3 (q, *Ar*), 136.4 (q, *Ar*), 138.9 (q, *Ar*), 142.9 (CH, C_{CN}), 147.1 (q, *Ar*), 154.3 (q, *Ar*), 164.8 (q, C_{CO}), ppm; HRMS: $C_{18}H_{14}N_3O_2$ $[M^+ + Na]$ requires (*m*/*e*) 392.0414, found 392.0413; HPLC Purity: 95%.

Time-Resolved Fluorescence Resonance Energy Transfer. Lanthascreen TR-FRET AR Coactivator Assay kit (Invitrogen, cat no. PV4381) was used to screen for potential coactivator disruptors. All compounds were prepared as 10 mM or 20 mM stocks in 100% DMSO and stored in −20 °C freezer. Black low volume 384-wells assay plates (Corning, NY, cat no. 3676) were used to perform the assay (total volume 20 μL) and TR FRET signal measured with PHERAstar equipment (BMG LabTech) using a Lanthascreen optic module excitation 335 nm, emission 520 nm-channel A and 495 nm-channel B. TR FRET values were calculated at ten flashes per well, using a delay time of 100 μs and an integration time of 200 μs as recommended by the Invitrogen assay guidelines. The ratio 520 nm/495 nm was then calculated and plotted against the concentration. A serial dilution of compounds was first prepared in 100X DMSO (Sigma-Aldrich) starting from the maximum desired concentration to achieve a 12 point range concentration using 96-well polypropylene plates (Nalgene Nunc, Rochester, NY). Each 100X solution was diluted to 2X concentration with TR-FRET coregulator buffer A (Invitrogen proprietary buffer), yielding a final concentration of 1% DMSO in each well. 10 μL of 2X solution was then added to the 384 well plate, following addition of 5 μL of 4x AR-LBD and 5 μL of D11-FXXLF/Tb Anti-GST antibody in agonist mode and 5 μL of D11-FXXLF/Tb anti-GST antibody/DHT (included at a concentration equal to EC_{80} as determined by running the assay in agonist mode first).

$$EC_{80} = 10((\log EC_{50}) + ((1/\text{Hill Slope}) \times \log(80/(100\text{-}80)))$$

D11-FXXLF and Tb antibody were premixed in light protecting vials prior to use. A final concentration of DTT 5 mM was used in the assay buffer in order to prevent protein degradation. All plates (agonist and antagonist mode) were incubated between 2 and 4 h at room temperature protected from light prior to TR-FRET measurement. IC_{50} values were determined by testing each ligand at concentrations ranging from 100 μM to 45 nM using 2-fold and 3-fold dilutions to generate a 12 point dose response curve. Data were fitted using the sigmoidal dose response (variable slope) available from Graphpad Prism 5.[42]

$$Y = \text{Bottom} + (\text{Top-Bottom}) /(1 + 10((\text{LogIC}_{50}\text{-X})*\text{HillSlope}))$$

The *Z′* factor for these assays was >0.5 as calculated by the equation provided by Zhang et al.[43]

In line with the assay protocol, a known agonist, dihydrotestosterone (DHT, cat no. A8380, Sigma), and a known antagonist, cyproterone acetate (cat no. C3412, Sigma), were used as controls in the assay. A control with no AR-LBD present was included to account for diffusion enhanced FRET or ligand-independent coactivator recruitment. A negative control with 2X DMSO was present to account for any solvent vehicle effects. (The protocol was also repeated including 0.01% Triton X-100 in the assay buffer to exclude an aggregation/nonspecific mechanism of inhibition).

Fluorescence Polarization. PolarScreen TM Androgen Receptor Competitor Assay Kit Green (Invitrogen, cat no. P3018) was used to investigate the binding of the test compound to the LBP site, occupied by a high affinity fluorophore ligand (Fluormone TM). 100X test compound solutions in DMSO were diluted in AR green buffer (Invitrogen) to achieve 2X concentrations and placed in a 384 well plate (Corning, cat no. 3576) with 40 μL volume capacity. AR-LBD was supplemented with 5 mM DTT to prevent protein degradation. AR-LBD and Fluormone (2X) mix are prepared separately and then added to each compound dilution to achieve a final concentration LBD-Fluormone of 50 nM and 2 nM, respectively. Plates were incubated while protected from light for at least 4 h. Controls included a maximum mP positive control, which consists of the AR-LBD and Fluormone mix (2X), and a minimum mP control, containing only Fluormone (2X). A vehicle control was added to account for DMSO effect, and a blank control containing buffer only. Fluorescence polarization was measured with PHERAstar equipment (BMG LabTech) using an optic module with excitation at 485 nm and emission at 530 nm.

Theoretical Study. *Docking Studies of Structures **46, 27, 47, 28, 22,** and **41**.* Structure data were read from the PDB reference 1T73 containing the crystal structure of the androgen receptor ligand binding domain in complex with a FXXLF motif. Completion of missing atoms and prepreparation of the protein was performed with MOE, optimization of the hydrogen bond network and calculation of the charges was made using 'Protonate 3D' and 'Partial Charges' implemented in MOE using default parameters. Ligand conformations were generated with a 'LowModeMD Search' method as implemented in MOE. The placement of the ligand within the site was guided by introducing three pharmacophoric constraints (aromatic/hydrophobic) into the three subpockets mimicking the protein:coactivator interaction. Docking was performed by using the 'Induce Fit' protocol. Affinity DG function was used for scoring and AMBER 99 forcefield for the refinement of the poses (MOE).

*Minimization and MMPBSA Single Point Binding Energy of Structures **46, 27, 47, 28, 22, and 41***. The docked poses were energy-minimized by using the AMBER software.[44] The ff99SB[45] and GAFF[46] force fields were utilized for building the protein and the ligands, respectively. Systems were solvated adding a water explicit box with a minimum distance between any atom of our molecule and the edge of the box of 12 Å.[47] The minimizations were carried out in a multistep procedure restraining with a harmonic potential of force constant of 10, 5, 1, and 0.1 kcal/mol^2 Å^2, respectively. Finally, complexes were minimized without any restriction. The MMPBSA approach was applied to minimized poses providing 'single point' binding energies (Poisson−Boltzmann, PB).

*Molecular Dynamic Simulation and Energy Analysis of Compounds **46, 27, 47, 28, 22, and 41***. After minimization, the selected complexes were gradually heated in the NVT ensemble (constant volume and temperature conditions) from 0 to 300 K. Then, the systems were equilibrated for 50 ps at a constant temperature of 300 K by coupling the system to a thermal bath with Berendsen algorithm with a time coupling constant of 1 ps and a pressure of 1 atm (NPT).[48] Systems were then simulated in the NVT ensemble for 40 ns. For the stable complexes, the last 5 ns of production step were used for further energy analysis. Binding free energies were calculated using the molecular mechanics Poisson−Boltzmann surface area (MMPBSA)[49] as implemented in AMBER. Finally, Pairwise Free Energy Decomposition Analysis was performed to identify the key residues in the binding mode of our proposed most probable bioactive conformation.

■ ASSOCIATED CONTENT

Ⓢ Supporting Information

NMR spectra (^{1}H NMR and ^{13}C NMR) and DELTA G binding graphs (Production Dynamics). This material is available free of charge via the Internet at http://pubs.acs.org.

■ AUTHOR INFORMATION

Corresponding Author

*Phone: +353 1 896 2904. Fax: +353 1 677 2400. E-mail: blancof@tcd (F.B.), david.lloyd@unisa.edu.au (D.G.L.).

Notes

The authors declare no competing financial interest.

The authors declare no competing financial interest.

■ ACKNOWLEDGMENTS

The authors thank the Irish Health Research Board (HRB) (HRB/2007/2), Enterprise Ireland (EI- CFTD/06/110) for research funding. The Trinity Biomedical Sciences Institute is supported a capital infrastructure investment from Cycle 5 of the Irish Higher Education Authority's Programme for Research in Third Level Institutions (PRTLI). F.B. thanks the support of the European Commission (Marie-Curie grant, People FP7, Project Reference: 274988). Molecular Dynamics simulations were performed on the Stoney cluster maintained by the Irish Centre for High-End Computing (ICHEC). We would like to thank Dr. Martin Peters for his assistance.

■ ABBREVIATIONS USED

AF-2, activation function-2; AMBER, assisted model building with energy refinement; AR, androgen receptor; ADT, androgen deprivation therapy; CPA, cyproterone acetate; CPRC, castration resistant prostate cancer; DHT, dihydrotestosterone; DMSO, dimethyl sulfoxide; FP, fluorescence polarization; HB, hydrogen bond; IMHB, intramolecular hydrogen bond; LBD, ligand binding domain; LBP, ligand binding pocket; MD, molecular dynamics; MMPBSA, molecular mechanics/Poisson−Boltzmann surface area; NB, nuclear box; NR, nuclear receptor; ns, nanoseconds; EPB, Poisson−Boltzmann energy binding; P, pose; SAR, structure−activity relationship; sp, single point; SBMA, spinal bulbar muscular atrophy; SRC, steroid receptor coactivator; S, subpocket; T, testosterone; TR-FRET, time resolved fluorescence resonance energy transfer; *wt*, wild type

■ REFERENCES

(1) Jemal, A.; Siegel, R.; Ward, E.; Hao, Y.; Xu, J.; Murray, T.; Thun, M. J. Cancer statistics, 2008. *Ca-Cancer J. Clin.* **2008**, *58*, 71-96.

(2) Huggins, C.; Hodges, C. V. Studies on prostatic cancer. I. The effect of castration, of estrogen and androgen injection on serum phosphatases in metastatic carcinoma of the prostate. *Ca-Cancer J. Clin.* **1972**, *22*, 232−240.

(3) Heinlein, C. A.; Chang, C. Androgen receptor in prostate cancer. *Endocr. Rev.* **2004**, *25*, 276−308.

(4) Evans, R. M. The steroid and thyroid hormone receptor superfamily. *Science* **1988**, *240*, 889−895.

(5) He, B.; Kemppainen, J. A.; Voegel, J. J.; Gronemeyer, H.; Wilson, E. M. Activation function 2 in the human androgen receptor ligand binding domain mediates interdomain communication with the NH(2)-terminal domain. *J. Biol. Chem.* **1999**, *274*, 37219−37225.

(6) Heemers, H. V.; Tindall, D. J. Androgen receptor (AR) coregulators: a diversity of functions converging on and regulating the AR transcriptional complex. *Endocr. Rev.* **2007**, *28*, 778−808.

(7) Taplin, M. E.; Balk, S. P. Androgen receptor: a key molecule in the progression of prostate cancer to hormone independence. *J. Cell. Biochem.* **2004**, *91*, 483−490.

(8) Heinlein, C. A.; Chang, C. Androgen receptor (AR) coregulators: an overview. *Endocr. Rev.* **2002**, *23*, 175−200.

(9) MOE. 2010.10; Chemical Computing Group: Montreal, 2010. www.chemcomp.com (accessed January 2013).

(10) Gomella, L. G.; Singh, J.; Lallas, C.; Trabulsi, E. J. Hormone therapy in the management of prostate cancer: evidence-based approaches. *Ther. Adv. Urol.* **2010**, *2*, 171−181.

(11) Feldman, B. J.; Feldman, D. The development of androgen-independent prostate cancer. *Nat. Rev. Cancer* **2001**, *1*, 34−45.

(12) Chen, C. D.; Welsbie, D. S.; Tran, C.; Baek, S. H.; Chen, R.; Vessella, R.; Rosenfeld, M. G.; Sawyers, C. L. Molecular determinants of resistance to antiandrogen therapy. *Nat. Med.* **2004**, *10*, 33−39.

(13) Kawata, H.; Arai, S.; Nakagawa, T.; Ishikura, N.; Nishimoto, A.; Yoshino, H.; Shiraishi, T.; Tachibana, K.; Nakamura, R.; Sato, H. Biological properties of androgen receptor pure antagonist for treatment of castration-resistant prostate cancer: optimization from lead compound to CH5137291. *Prostate* **2011**, *71*, 1344−1356.

(14) Sharifi, N. New agents and strategies for the hormonal treatment of castration-resistant prostate cancer. *Expert Opin. Invest. Drugs* **2010**, *19*, 837−846.

(15) Tran, C.; Ouk, S.; Clegg, N. J.; Chen, Y.; Watson, P. A.; Arora, V.; Wongvipat, J.; Smith-Jones, P. M.; Yoo, D.; Kwon, A.; Wasielewska, T.; Welsbie, D.; Chen, C. D.; Higano, C. S.; Beer, T. M.; Hung, D. T.; Scher, H. I.; Jung, M. E.; Sawyers, C. L. Development of a second-generation antiandrogen for treatment of advanced prostate cancer. *Science* **2009**, *324*, 787−790.

(16) Scher, H. I.; Beer, T. M.; Higano, C. S.; Anand, A.; Taplin, M. E.; Efstathiou, E.; Rathkopf, D.; Shelkey, J.; Yu, E. Y.; Alumkal, J.; Hung, D.; Hirmand, M.; Seely, L.; Morris, M. J.; Danila, D. C.; Humm, J.; Larson, S.; Fleisher, M.; Sawyers, C. L. Antitumour activity of MDV3100 in castration-resistant prostate cancer: a phase 1−2 study. *Lancet* **2010**, *375*, 1437−1446.

(17) Jung, M. E.; Ouk, S.; Yoo, D.; Sawyers, C. L.; Chen, C.; Tran, C.; Wongvipat, J. Structure-activity relationship for thiohydantoin

androgen receptor antagonists for castration-resistant prostate cancer (CRPC). *J. Med. Chem.* **2010**, *53*, 2779−2796.
(18) Attar, R. M.; Jure-Kunkel, M.; Balog, A.; Cvijic, M. E.; Dell-John, J.; Rizzo, C. A.; Schweizer, L.; Spires, T. E.; Platero, J. S.; Obermeier, M.; Shan, W.; Salvati, M. E.; Foster, W. R.; Dinchuk, J.; Chen, S. J.; Vite, G.; Kramer, R.; Gottardis, M. M. Discovery of BMS-641988, a novel and potent inhibitor of androgen receptor signaling for the treatment of prostate cancer. *Cancer Res.* **2009**, *69*, 6522−6530.
(19) Rathkopf, D.; Liu, G.; Carducci, M. A.; Eisenberger, M. A.; Anand, A.; Morris, M. J.; Slovin, S. F.; Sasaki, Y.; Takahashi, S.; Ozono, S.; Fung, N. K.; Cheng, S.; Gan, J.; Gottardis, M.; Obermeier, M. T.; Reddy, J.; Zhang, S.; Vakkalagadda, B. J.; Alland, L.; Wilding, G.; Scher, H. I. Phase I dose-escalation study of the novel antiandrogen BMS-641988 in patients with castration-resistant prostate cancer. *Clin. Cancer Res.* **2011**, *17*, 880−887.
(20) Clegg, N. J.; Wongvipat, J.; Tran, C.; Ouk, S.; Dilhas, A.; Joseph, J.; Chen, Y.; Grillot, K.; Bischoff, E. D.; Cai, L.; Aparicio, A.; Dorow, S.; Arora, V.; Shao, G.; Qian, J.; Zhao, H.; Yang, G.; Cao, C.; Sensintaffar, J.; Wasielewska, T.; Herbert, M. R.; Bonnefous, C.; Darimont, B.; Scher, H. I.; Smith-Jones, P. M.; Klang, M.; Smith, N. D.; de Stanchina, E.; Wu, N.; Ouerfelli, O.; Rix, P.; Heyman, R.; Jung, M. E.; Sawyers, C. L.; Hager, J. H. ARN-509: a novel anti-androgen for prostate cancer treatment. *Cancer Res.* **2012**, *72*, 1494−1503.
(21) Estebanez-Perpina, E.; Arnold, L. A.; Nguyen, P.; Rodrigues, E. D.; Mar, E.; Bateman, R.; Pallai, P.; Shokat, K. M.; Baxter, J. D.; Guy, R. K.; Webb, P.; Fletterick, R. J. A surface on the androgen receptor that allosterically regulates coactivator binding. *Proc. Natl. Acad. Sci. U.S.A.* **2007**, *104*, 16074−16079.
(22) Buzon, V.; Carbo, L. R.; Estruch, S. B.; Fletterick, R. J.; Estebanez-Perpina, E. A conserved surface on the ligand binding domain of nuclear receptors for allosteric control. *Mol. Cell. Endocrinol.* **2011**, *348*, 394−402.
(23) Moore, T. W.; Mayne, C. G.; Katzenellenbogen, J. A. Minireview: Not picking pockets: nuclear receptor alternate-site modulators (NRAMs). *Mol. Endocrinol.* **2009**, *24*, 683−695.
(24) Estebanez-Perpina, E.; Jouravel, N.; Fletterick, R. J. Perspectives on designs of antiandrogens for prostate cancer. *Expert Opin. Drug Discovery* **2007**, *2*, 1341−1355.
(25) Chang, C. Y.; McDonnell, D. P. Androgen receptor-cofactor interactions as targets for new drug discovery. *Trends Pharmacol. Sci.* **2005**, *26*, 225−228.
(26) Gunther, J. R.; Parent, A. A.; Katzenellenbogen, J. A. Alternative inhibition of androgen receptor signaling: peptidomimetic pyrimidines as direct androgen receptor/coactivator disruptors. *ACS Chem. Biol.* **2009**, *4*, 435−440.
(27) Axerio-Cilies, P.; Lack, N. A.; Nayana, M. R.; Chan, K. H.; Yeung, A.; Leblanc, E.; Guns, E. S.; Rennie, P. S.; Cherkasov, A. Inhibitors of androgen receptor activation function-2 (AF2) site identified through virtual screening. *J. Med. Chem.* **2011**, *54*, 6197−6205.
(28) Lack, N. A.; Axerio-Cilies, P.; Tavassoli, P.; Han, F. Q.; Chan, K. H.; Feau, C.; LeBlanc, E.; Guns, E. T.; Guy, R. K.; Rennie, P. S.; Cherkasov, A. Targeting the binding function 3 (BF3) site of the human androgen receptor through virtual screening. *J. Med. Chem.* **2011**, *54*, 8563−8573.
(29) Sadar, M. D. Small molecule inhibitors targeting the "achilles' heel" of androgen receptor activity. *Cancer Res.* **2011**, *71*, 1208−1213.
(30) Chang, C. Y.; Abdo, J.; Hartney, T.; McDonnell, D. P. Development of peptide antagonists for the androgen receptor using combinatorial peptide phage display. *Mol. Endocrinol.* **2005**, *19*, 2478−2490.
(31) Dominguez-Seoane, M.; Petkau-Milroy, K.; Vaz, B.; Möcklinghoff, S.; Folkertsma, S.; Milroy, L. G.; Brunsveld, L. Structure−activity relationship studies of miniproteins targeting the androgen receptor−coactivator interaction *Med. Chem. Commun.* **2013**, *4*, 187−192.
(32) Munuganti, R. S. N.; Leblanc, E.; Axerio-Cilies, P.; Labriere, Ch.; Frewin, K.; Hassona, M. D. H.; Lack, N. A.; Li, H.; Ban, F.; Guns, E. T.; Young, R.; Rennie, P. S.; Cherkasov, A. Targeting the binding function 3 (BF3) site of the androgen receptor through virtual screening. 2. Development of 2-((2-phenoxyethyl) thio)-1H-benzimidazole derivatives. *J. Med. Chem.* **2013**, *56*, 1136−1148.
(33) Caboni, L.; Kinsella, G. K.; Blanco, F.; Fayne, D.; Jagoe, W. N.; Carr, M.; Williams, D. C.; Meegan, M. J.; Lloyd, D. G. 'True' antiandrogens - selective non ligand-binding pocket disruptors of androgen receptor-coactivator interactions: Novel tools for prostate cancer. *J. Med. Chem.* **2012**, *55*, 1635−1644.
(34) Blanco, F.; Egan, B.; Caboni, L.; Elguero, J.; O'Brien, J.; McCabe, T.; Fayne, D.; Meegan, M. J.; Lloyd, D. G. Study of E/Z isomerization in a series of novel non-ligand binding pocket androgen receptor antagonists. *J. Chem. Inf. Model.* **2012**, *52*, 2387−2397.
(35) McKenna, N. J.; O'Malley, B. W. Minireview: Nuclear receptor coactivators–an update. *Endocrinology* **2002**, *143*, 2461−2465.
(36) Hur, E.; Pfaff, S. J.; Payne, E. S.; Gron, H.; Buehrer, B. M.; Fletterick, R. J. Recognition and accommodation at the androgen receptor coactivator binding interface. *PLoS Biol.* **2004**, *2*, E274.
(37) He, B.; Gampe, R. T., Jr.; Kole, A. J.; Hnat, A. T.; Stanley, T. B.; An, G.; Stewart, E. L.; Kalman, R. I.; Minges, J. T.; Wilson, E. M. Structural basis for androgen receptor interdomain and coactivator interactions suggests a transition in nuclear receptor activation function dominance. *Mol. Cell* **2004**, *16*, 425−438.
(38) Gottlieb, H. E.; Kotlyar, V.; Nudelman, A. NMR chemical shifts of common laboratory solvents as trace impurities. *J. Org. Chem.* **1997**, *62*, 7512−7515.
(39) Franzen, H. Replacement of hydroxyl by the hydrazine group. *J. Prakt. Chem.* **1909**, *78*, 157−164.
(40) Ganjali, M. R. Nano-level monitoring of ytterbium(III) by a novel ytterbium(III) membrane sensor based on 3-hydroxy-N′-[(2-hydroxyphenyl) methylene]-2-naphthohydrazide. *Sensor. Actuat. B-Chem.* **2006**, *114*, 855−860.
(41) Monfared, H. H. Homogeneous green catalysts for olefin oxidation by mono oxovanadium(V) complexes of hydrazone Schiff base ligands. *Inorg. Chim. Acta* **2010**, *363*, 2574−2583.
(42) *Prism* 5.01; GraphPad Software: San Diego, CA. www.graphpad.com (accessed January 2013).
(43) Zhang, J. H.; Chung, T. D.; Oldenburg, K. R. A simple statistical parameter for use in evaluation and validation of high throughput screening assays. *J. Biomol. Screening* **1999**, *4*, 67−73.
(44) Case, D. A.; Darden, T. A.; Cheatham, T. E., III; Simmerling, C. L.; Wang, J.; Duke, R. E.; Luo, R.; Walker, R. C.; Zhang, W.; Merz, K. M.; Roberts, B.; Wang, B.; Hayik, S.; Roitberg, A.; Seabra, G.; Kolossváry, I.; Wong, K. F.; Paesani, F.; Vanicek, J.; Wu, X.; Brozell, S. R.; Steinbrecher, T.; Gohlke, H.; Cai, Q.; Ye, X.; Wang, J.; Hsieh, M.-J.; Cui, G.; Roe, D. R.; Mathews, D. H.; Seetin, M. G.; Sagui, C.; Babin, V.; Luchko, T.; Gusarov, S.; Kovalenko, A.; Kollman P. A. *AMBER* 11; University of California: San Francisco, 2010.
(45) Duan, Y.; Wu, C.; Chowdhury, S.; Lee, M. C.; Xiong, G.; Zhang, W.; Yang, R.; Cieplak, P.; Luo, R.; Lee, T. A point-charge force field for molecular mechanics simulations of proteins based on condensed-phase quantum mechanical calculations. *J. Comput. Chem.* **2003**, *24*, 1999−2012.
(46) Wang, J.; Wolf, R. M.; Caldwell, J. W.; Kollman, P. A.; Case, D. A. Development and testing of a general amber force field. *J. Comput. Chem.* **2004**, *25*, 1157−1174.
(47) Jorgensen, W. L.; Chandrasekhar, J.; Madura, J. D.; Impey, R. W.; Klein, M. L. Comparison of simple potential functions for simulating liquid water. *J. Chem. Phys.* **1983**, *79*, 926−935.
(48) Berendsen, H. J. C.; Postma, J. P. M.; Vangunsteren, W. F.; Dinola, A.; Haak, J. R. Molecular-dynamics with coupling to an external bath. *J. Chem. Phys.* **1984**, *81*, 3684−3690.
(49) Kollman, P. A.; Massova, I.; Reyes, C.; Kuhn, B.; Huo, S.; Chong, L.; Lee, M.; Lee, T.; Duan, Y.; Wang, W.; Donini, O.; Cieplak, P.; Srinivasan, J.; Case, D. A.; Cheatham, T. E., III Calculating structures and free energies of complex molecules: combining molecular mechanics and continuum models. *Acc. Chem. Res.* **2000**, *33*, 889−897.